Formation and impacts of nitryl chloride in Pearl River Delta

Haichao Wang[1,4], Bin Yuan[2,3,*], E Zheng[2,3], Xiaoxiao Zhang[2,3], Jie Wang[1], Keding Lu[5,6], Chenshuo Ye[2,3], Lei Yang[2,3], Shan Huang[2,3], Weiwei Hu[7], Suxia Yang[2,3], Yuwen Peng[2,3], Jipeng Qi[2,3], Sihang Wang[2,3], Xianjun He[2,3], Yubin Chen[2,3], Tiange Li[2,3], Wenjie Wang[2,8], Yibo Huangfu[2,3], Xiaobing Li[2,3], Mingfu Cai[2,3], Xuemei Wang[2,3], Min Shao[2,3]

[1] *School of Atmospheric Sciences, Sun Yat-sen University, Zhuhai, 519082, China*

[2] *Institute for Environmental and Climate Research, Jinan University, Guangzhou 511443, China*

[3] *Guangdong–Hong Kong–Macau Joint Laboratory of Collaborative Innovation for Environmental Quality, Guangzhou, 511443, China*

[4] *Guangdong Provincial Observation and Research Station for Climate Environment and Air Quality Change in the Pearl River Estuary, Key Laboratory of Tropical Atmosphere-Ocean System, Ministry of Education, Southern Marine Science and Engineering Guangdong Laboratory (Zhuhai), Zhuhai, 519082, China*

[5] *State Key Joint Laboratory of Environmental Simulation and Pollution Control, College of Environmental Sciences and Engineering, Peking University, Beijing, 100871, China.*

[6] *The State Environmental Protection Key Laboratory of Atmospheric Ozone Pollution Control, College of Environmental Sciences and Engineering, Peking University, Beijing, 100871, China*

[7] *State Key Laboratory of Organic Geochemistry and Guangdong Key Laboratory of Environmental Protection and Resources Utilization, Guangzhou Institute of Geochemistry, Chinese Academy of Sciences, Guangzhou 510640, China*

[8] *Multiphase Chemistry Department, Max Planck Institute for Chemistry, Mainz 55128, Germany*

Correspondence: Bin Yuan (byuan@jnu.edu.cn)

Abstract. Here we present a field measurement of $ClNO_2$ (nitryl chloride) and N_2O_5 (dinitrogen pentoxide) by a Time-of-Flight Chemical Ionization Mass Spectrometer (ToF-CIMS) with the Filter Inlet for Gas and AEROsols (FIGAERO) at a regional site in Pearl River Delta during a photochemical pollution season from Sept. 26th to Nov. 17th, 2019. Three patterns of air masses are sampled during this campaign, including the dominating air masses from the north and northeast urban regions (Type A), the southeast coast (Type B), and the South China Sea (Type C). The concentration of $ClNO_2$ and N_2O_5 were observed to be much higher in Type A and B than ~~those in Type C, indicated~~ in Type C, indicating that the urban nighttime chemistry is more active than the background marine regions. N_2O_5 uptake coefficient and $ClNO_2$ production yield were estimated ~~by measured parameters~~ based on the field measurement, and the performance of the previously derived parameterizations ~~were~~ was assessed~~.~~. The nighttime $ClNO_2$ correlated with particulate chloride and the mass concentration of fine particles (most likely due to aerosol surface area), ~~but not with nitrate radical formation rate,~~ suggested that the $ClNO_2$ formation was limited by the N_2O_5 uptake ~~rather than N_2O_5 source~~ at this site. By examining the relationship ~~of~~ between particulate chloride and other species, we implied that anthropogenic emissions (e.g., biomass burning) rather than sea salt particles dominate the origin of particulate chloride, ~~despite~~ although the site ~~i~~ being only about 100 km away from the ocean. A box model with detailed ~~chloride chemistry~~ chlorine chemistry is used to investigate the impacts of $ClNO_2$ chemistry on atmospheric oxidation. Model simulations showed the ~~chloride radical~~ chlorine radical liberated by $ClNO_2$ photolysis during the next day had a ~~small~~ slight increase in concentrations of OH, HO_2 and RO_2 radicals, as well as minor contributions to RO_2 radical and O_3 formation (<5%, on daytime average) in all the three types of air masses. Relative higher contributions were observed in Type A and B. The overall low contributions of $ClNO_2$ to atmospheric oxidation are consistent with those reported recently from wintertime observations in China (~~included~~ including Shanghai, Beijing, Wangdu and Mt. Tai). This may be attributed to: (1) Relative low particle mass concentration limited $ClNO_2$ formation; (2) Other reactions channels, like nitrous acid (HONO), oxygenated volatile organic compounds (OVOCs, including formaldehyde), and ozone photolysis, had ~~larger~~ more significant radical formation rate during the ozone pollution episodes and weakened the $ClNO_2$ contribution indirectly. The results provided scientific insights into the role of nighttime chemistry in photochemical pollution under various scenarios in coastal areas.

1. Introduction

~~Chloride radical~~Chlorine radical is an important oxidant in the tropospheric besides OH radicals, NO_3 radicals and ozone (Saiz-Lopez and von Glasow, 2012; Simpson et al., 2015; Wang et al., 2019b), which alters the fate of many atmospheric compositions, including oxidants, reactive nitrogen compounds, volatile organic compounds (VOCs), and other halogens. Cl radical is much more reactive than OH ~~with respect to~~concerning certain VOCs (e.g., alkanes) by a few orders of magnitude for reaction rate constant (Atkinson and Arey, 2003; Atkinson et al., 2006)~~,~~ therefore, it contributes to atmospheric oxidation capacity considerably in the troposphere despite low concentrations. For example, the global model showed ~~–~~about 20 % of ethane, 14 % of propane oxidation are attributed to ~~the chloride chemistry~~chlorine chemistry at the global scale (Wang et al., 2019c). Modeling simulations also demonstrated that ~~chloride chemistry~~chlorine chemistry enhanced oxidative degradation of VOCs by >20% at some locations (Sarwar et al., 2014).

Photolysis of $ClNO_2$ (R1) is a major source of the tropospheric ~~chloride radical~~chlorine radical (Thornton et al., 2010b; Simpson et al., 2015), other ~~chloride radical~~chlorine radical sources include the reaction of HCl with OH (Riedel et al., 2012; Eger et al., 2019), photolysis of Cl_2 and other halogen compounds like ICl and BrCl (Peng et al., 2021). Tropospheric $ClNO_2$ is not only ~~an important~~a critical chlorine activation precursor but also a nocturnal ~~resourvior~~reservoir of reactive nitrogen, which is mainly formed ~~in~~by N_2O_5 heterogeneous reaction ~~of N_2O_5~~ on chlorine-containing particles with a ~~branch~~branching ratio at nighttime (R2).

$$ClNO_2 + hv \rightarrow Cl + NO_2 \qquad (R1)$$

$$N_2O_5 + H_2O/Cl^- \rightarrow \varphi ClNO_2 + (2-\varphi)NO_3^- \quad (R2)$$
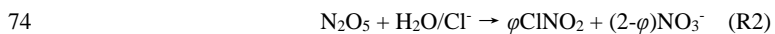
where φ represents the yield of $ClNO_2$. This mechanism was firstly proposed by Finlaysonpitts et al. (1989) through detecting the products of N_2O_5 uptake on NaCl particles. Given this reaction, the formation of $ClNO_2$ can be influenced by the N_2O_5 uptake (such as N_2O_5 uptake probabilities and aerosol surface area) as well as the production yield of $ClNO_2$.

N_2O_5 uptake coefficient, $\gamma(N_2O_5)$, have been reported highly varied under tropospheric conditions (Brown and Stutz, 2012). Both the field and laboratory studies revealed that this process can be affected by ambient temperature, relative humidity (Mozurkewich and Calvert, 1988; Mentel et al., 1999; Hallquist et al., 2003), chemical compositions (such as the content of nitrate, liquid water, chloride, and organics) (Mentel et al., 1999; Brown et al., 2006; Bertram and Thornton, 2009; Gaston

et al., 2014; McDuffie et al., 2018b; Tang et al., 2014; Anttila et al., 2006), as well as particle morphology (Mielke et al., 2013; Zong et al., 2021). Until now, the key factors that controlling N_2O_5 uptake coefficient in the different environments are still not well understood. $ClNO_2$ yield is also highly varied subject to the liquid water and chloride content in the aerosol (Behnke et al., 1997; Roberts et al., 2009; Bertram and Thornton, 2009). Several studies demonstrated that the $ClNO_2$ yield is also affected by other factors like aerosol sulfate (Staudt et al., 2019) and organics (Ryder et al., 2015; Tham et al., 2018; McDuffie et al., 2018a). However, the comprehensive quantitative relationship of these factors in controlling the yield still has large uncertainties. These gaps in parameterization of N_2O_5 uptake coefficients and $ClNO_2$ yield result in challenging to accurately predict $ClNO_2$ and particulate nitrate production.These gaps in understanding the critical controlling factors for N_2O_5 uptake coefficient as well as $ClNO_2$ yield lead to the prediction of $ClNO_2$ and particulate nitrate production very challenge.

Osthoff et al. (2008) and Thornton et al. (2010a) directly observed elevated $ClNO_2$ in coastal and inland U.S. by chemical ionization mass spectrometer (CIMS), respecitively. They shed light on the significance of $ClNO_2$ photolysis in launching the radical chemistry during the morning time, and also affecting halogen chemistry and reactive nitrogen cycling. Large amounts of chloride radicalchlorine radicals are liberated through the photolysis of noctural accumulated $ClNO_2$ (R1), which oxidizes VOCs and produces peroxy radicals (RO_2) to initiate the daytime raidcal cycling in the morning, when other radical source, like ozonolysis and photolysis of O_3, HONO and HCHO, are still weak (Osthoff et al., 2008). The impacts of $ClNO_2$ chemistry on primany source of radicals and ozone formation is a critical topic, the answer of which is very helpful to narrow the gap of the missing priamry source of ROx and improve our knowledge of the currect ozone pollution mechanism (Tan et al., 2017; Tham et al., 2016). Model simulation highlighted $ClNO_2$ chemistry could increase mean daily maximum 8 h ozone by up to 7.0 ppbv in some areas in the Northern Hemisphere (Sarwar et al., 2014). The large contribution was also confirmed in the southern California region by a box model study (Riedel et al., 2014). In addition, global model simualtion showed $ClNO_2$ chemistry increases wintertime ozone by up to 8 ppb over polluted continents (Wang et al., 2019c). Particularly, previously modelling results also highlight the importance of $ClNO_2$ chemistry in enhancing O_3 production in China (Li et al., 2016; Yang et al., 2022b).

Several field studies reported the measurement of $ClNO_2$ in varied environments in the past decade (Riedel et al., 2012; Young et al., 2012; Mielke et al., 2013; Riedel et al., 2013; Bannan et al., 2015; Faxon et al., 2015; Mielke et al., 2015; Phillips et al., 2016; Bannan et al., 2017; Wang et al., 2017c; Wang et al., 2017d; Le Breton et al., 2018; McDuffie et al., 2018a; Yun et al., 2018a; Zhou et al., 2018; Bannan et al., 2019; Eger et al., 2019; Haskins et al., 2019; Jeong et al., 2019; Xia et al.,

118 2020; Xia et al., 2021; Tham et al., 2016; Tham et al., 2014; Wang et al., 2016; Phillips et al., 2012;

119 Lou et al., 2022; Sommariva et al., 2018), in which the maximum $ClNO_2$ up to sub-ppbv to several

120 ppbv were reported, indicating its ubiquitous~~ubiquity~~ presence worldwide and a broad atmospheric

121 impacts over various regions. During the CalNex-LA campaign 2010, $ClNO_2$ was measurred at

122 ground site, the Research Vessel and aircraft platform, which depicted a full picture of the abundance

123 of $ClNO_2$ and confirmed its large impacts on atmospheric chemsitry in both urban and coastal

124 regions in California (Riedel et al., 2012; Young et al., 2012; Mielke et al., 2013). Recently, Wang et

125 al. (2016) used a box model simulated the chemical evolution of the plume after leaving the

126 observation site in Hongkong and showed $ClNO_2$ chemistry had a following-day enhancement of

127 ozone peak and daytime ozone production rate by 5–16% and 11–41%, along with a large increasing

128 of OH, HO_2 and RO_2 concentration especially in the morning. While Xia et al. (2021) and Lou et al.

129 (2022) reported winter measurments of $ClNO_2$ in north and east China, respectively, ~~both~~ they both

130 showed moderate $ClNO_2$ level and a relative small contributions of $ClNO_2$ chemistry to radical

131 source and ozone enhancement on campaign average. These results is quite different with that

132 happened during the summertime in China (Tham et al., 2016; Wang et al., 2016; Tan et al., 2017),

133 and highlight the large variation of $ClNO_2$ chemistry influenced by temporal spatial distribution.

134   Despite its likely importance to the regional atmospheric oxidation and air quality, investigations

135 of $ClNO_2$ chemistry in China remain relatively sparse. There are several field measurements of

136 $ClNO_2$ conducted in the China in recent years, while considering the large diversities of air mass in

137 inland and coastal regions in China, more field and model works are need to gain more insights to

138 the $ClNO_2$ chemistry in various atmospheric environments and assess its atmospheric impacts. Until

139 now, only several field measurement of $ClNO_2$ were reported in Pearl River Delta (PRD) region

140 (Tham et al., 2014; Wang et al., 2016; Yun et al., 2018a), and only Wang et al. (2016) reported a

141 comprehensive analysis of the impact of $ClNO_2$ chemistry on radical and ozone formation in 2013 as

142 mentioned before. To understanding the increasing O_3 problem in recent years (Wang et al., 2019a)

143 and examining the role of $ClNO_2$ chemistry in O_3 formation in PRD, we measured $ClNO_2$, N_2O_5, and

144 other related parameters at a regional site in PRD during a severe photochemical pollution season in

145 2019. The abundance, formation, and variation during different air masses patterns are well

146 characterized. The factors impact its formation are diagnosed. Finally, the contribution of ~~chloride~~

147 ~~radical~~chlorine radicals liberated by $ClNO_2$ photolysis on the daytime radical chemistry, as well as

148 ozone formation are comprehensively assessed by a box model coupled with detailed ~~chloride~~

149 ~~chemistry~~chlorine chemistry.

150 **2. Method**

2.1 Measurement site

This campaign was conducted at the Guangdong Atmospheric Supersite of China, which is located on the top of a mountain (~ 60 m high, a.s.l.) in Heshan (22.728°N, 112.929°E), Jiangmen city, Guangdong Province (Yang et al., 2022a) . This site was in the western Peral River Delta where no major industry in the surroundings, but with some farmland and a few residents live at the hill foot. The traffic is far away from this site and believed to have little influence on the sampling. The anthropogenic activity is much lower than the urban regions like Guangzhou City, but the air quality is often influenced by neighbor cities, especially the outflow of air masses from the regions on the north and northeast. Therefore, the air masses sampled at this site are sometimes representative of the urban pollution from the center PRD. There were many atmospheric intensive studies once conducted in the site to study the air pollutions in PRD (Tan et al., 2019; Yun et al., 2018b). In this study, the instruments were located on the top floor of the measurement building with inlets approximately 15 m above the ground. The data presented in the study were collected from 27th September to 17th November 2019, during which photochemical pollution occurred frequently (Yang et al., 2022a). Time is given as CNST (Chinese National Standard Time = UTC+8 h). During the campaign, sunrise was approximately at 06:00 and sunset was approximately at 18:00 CNST.

2.2 Instrument setup

A comprehensive suite of instrumentation was overviewed and listed in Table 1. An iodide-adduct Time-of-Flight Chemical Ionization Mass Spectrometer (ToF-CIMS) with the Filter Inlet for Gas and AEROsols (FIGAERO) was applied to measure $ClNO_2$ and N_2O_5 along with other oxygenated organic species (Ye et al., 2021; Wang et al., 2020b) . In brief, the gas phase species were measured via a 2-m-long, 6-mm-outer-diameter PFA inlet while the particles were simultaneously collected on a Teflon filter via a separate 2-m-long, 10-mm-outer-diameter copper tubing inlet; both had flow rates of 2 L min^{-1} with a drainage flow of 20 L min^{-1}. The gas phase was measured for 25 minutes at 1 Hz, and the FIGAERO instrument was then switched to place the filter in front of the ion molecule region; it was then heated incrementally to 200 °C to desorb all the mass from the filter to be measured in the gas phase, which resulted in high-resolution thermograms. $ClNO_2$ and N_2O_5 are measured as the iodide adduct ions at m/z 207.867 ($IClNO_2^-$) and m/z 234.886 ($IN_2O_5^-$) in the ToF-CIMS, respectively. The measurement background and sensitivities for detecting $ClNO_2$ and N_2O_5 with the dependence of water content were quantified (see Appendix). The limit of detection (LOD) for $ClNO_2$ and N_2O_5 were 4.3 and 6.0 pptv in 1-minute time-resolution, respectively, with an uncertainty of ~30%.

184   Sub-micron aerosol composition (PM_1) were measured by a High-Resolution Time of Flight
185   Aerosol Mass Spectrometer (HR-ToF-AMS) (DeCarlo et al., 2006). The soluble ions of sodium and
186   potassium was measured by a commercial instrument (GAC-IC) equipped with an aerosol collector
187   and detected by ion chromatography (Dong et al., 2012). The particle number size distribution
188   (PNSD) was measured by a scanning mobility particle sizer (SMPS, TSI 3938). The aerosol surfaces
189   area was calculated based on the size distribution measurement and corrected to wet particle-state by
190   a hygroscopicity growth factor, with a total uncertainty of determining wet aerosol surface areas by
191   ~30% (Liu et al., 2013). VOCs were measured by Proton Transfer Reaction Time-of-Flight Mass
192   Spectrometry (PTR-MS)(Wu et al., 2020; He et al., 2022) and an automated gas chromatograph
193   equipped with mass spectrometry or flame ionization detectors (GC-MS). A commercial instrument
194   (Thermo Electron model 42i) was used to monitor NO_x. O_3 was measured by a commercial
195   instrument using ultraviolet (UV) absorption (Thermo Electron 49i). $PM_{2.5}$ was measured by a
196   Tapered Element Oscillating Microbalance (TEOM, 1400A analyzer). SO_2 and CO were measured
197   by commercial instruments (Thermo Electron 43i and 48i). In addition, the meteorological
198   parameters were available during the measurement. Photolysis frequencies were determined by a
199   spectroradiometer (Bohn et al., 2008). The aerosol liquid water content (ALWC) is calculated from
200   the ISORROPIA-II thermodynamic equilibrium model (Clegg et al., 1998). We used the reverse
201   mode in ISORROPIA-II with the input of water-soluble ions along with ambient temperature (T) and
202   relative humidity (RH). Given the high RH in this campaign, we ran the model by assuming aerosol
203   phase were metastable.

204   **Table 1.** Summary of the information about observed gas and particle parameters during the
205   campaign.

Species	Limit of detection	Methods	Accuracy
N_2O_5	6.0 pptv (3σ, 1 min)	FIGAERO-ToF-CIMS	± 30%
$ClNO_2$	4.3 pptv (3σ, 1 min)	FIGAERO-ToF-CIMS	± 30%
NO	60 pptv (2σ, 1 min)	Chemiluminescence	± 20%
NO_2	0.3 ppbv (2σ, 1 min)	Mo convert	± 20%
O_3	0.5 ppbv (2σ, 1 min)	UV photometry	± 5%
VOCs	0.1 ppbv (5 min)	PTR-ToF-MS	± 30%
VOCs	20-300 pptv (1 h)	GC-FID/MS	± 20%
$PM_{2.5}$	0.1 µg m − 3 (1 min)	TEOM	± 5%
CO	4 ppbv (5 min)	IR photometry	± 5%
SO_2	0.1 ppbv (1 min)	Pulsed UV fluorescence	± 10%
HCHO	25 pptv (2 min)	Hantzsch fluorimetry	± 5%
PNSD	14 nm -700 nm (4 min)	SMPS	± 20%
Aerosol composition	<0.16 µg m^{-3} (30 min)	GAC-IC	± 30%
PM_1 components	0.15 µg m^{-3} (4 min)	HR-ToF-AMS	± 30%
Photolysis frequencies	Varies with species (20 s)	Spectroradiometer	± 10%

206

2.3 Box model setup

A zero-dimensional chemical box model constrained by the field campaign data was applied to simulate the $ClNO_2$ chemistry. The box model was based on the Regional Atmospheric Chemical Mechanism version 2 (RACM2) described in Goliff et al. (2013), and ~~chloride~~ chlorine-related chemical mechanism ~~were~~was added (Wang et al., 2017b; Tan et al., 2017). Briefly, ~~chloride chemistry~~chlorine chemistry was adapted to RACM2 from the modifications to Master Chemical Mechanism (Xue et al., 2015), and the oxidation products from reactions between lumped VOC species and ~~chloride radical~~chlorine radicals were adapted from those of OH oxidation from RACM2. $j(ClNO_2)$ was calculated according to the NASA-JPL recommendation based on the work by Ghosh et al. (2012). The impact of O_3 by $ClNO_2$ chemistry was assessed by differing the results of two scenarios with and without the constrains of the observed $ClNO_2$~~with or without the constraints of the observed $ClNO_2$~~ in the model simulation. For the reaction rate constant of the lumped species with Cl, the fastest value from different species was used to represent the upper limit of the impact of ~~chloride chemistry~~chlorine chemistry. It should be note that the setting will lead to overestimation on the contributions from $ClNO_2$ chemistry. The model was constrained by the observed $ClNO_2$, NOx, O_3, CO, VOCs (assignment to RACM2), photolysis frequencies, ambient ~~temperature~~temperature, and pressure. The model runs were from 29 September to 17 November, 2019 with most of the measurement data taken accounted for, and with a two-days spin-up. The constant lifetime ~~of the input trace gases~~ corresponds to a deposition velocity of 1.2 cm s^{-1} with an assumed boundary layer height of 1000 m was used for the input trace gases, and the model-generated species ~~was~~were set to 24 hours lifetime due to the loss caused by the dry deposition (Lu et al., 2012). The input data were averaged and interpolated to 1 hour of resolution.

3. Results and discussions

3.1 Overview of measurement

Figure 1 shows time series of $ClNO_2$ and relevant trace gases, ~~particles~~particles, and meteorological parameters during the measurements. In this campaign, the meteorological condition featured high temperature (24.7 ± 3.8 ^{o}C) and high humidity (62.1% ± 15.6%), low wind speed (1.5 ± 0.8 m s^{-1}), and the dominant air flow were from north and northwest. Compared to those with previously

设置了格式: 下标

设置了格式: 下标

设置了格式: 上标

235 measurements at the same site in January 2017 (Yun et al., 2018b), the temperature was higher and
236 relative humidity was lower during the measurements. The average and maximum concentration of
237 particulate matter ($PM_{2.5}$) was 47.6±19.3 μg m^{-3} and 138 μg m^{-3}, respectively, which is significantly
238 lower than that observed in January 2017, with a maximum up to 400 μg m^{-3}. The dominant air
239 pollutant was O_3 with hourly campaign maximum and the average mean daily maximum 8-hour O_3
240 (MDA8 O_3) of 152.8 ppbv and 75.2 ±20.9 ppbv, respectively. There were 27 days out of 53 days
241 with the hourly maximum of O_3 exceeded the Chinese national air quality standard (200 μg m^{-3},
242 equivalent to 93 ppbv), suggesting severe ozone pollution during the measurement period in PRD
243 region. NO_2 concentration was also elevated with 21.0 ± 10.4 ppbv on campaign average. The
244 concurrent high O_3 and NO_2 made large nitrate radical production rate occurred with a daily average
245 of 2.5 ~~1.8±~~ 2.1 ppbv h^{-1} (median, 1.8 ppbv h^{-1}). The campaign maximum NO_3 production rate was
246 observed up to 18.6 ppbv h^{-1} in the afternoon at 11th November, 2019. At night, the nitrate radical
247 production rate was 1.8 ± 1.5 ppbv h^{-1} on campaign average (median, 1.4 ppbv h^{-1}). However, high
248 NO_3 production rate did not mean high concentrations of NO_3, N_2O_5 and $ClNO_2$ in the atmosphere,
249 as the concentration affected by both their sources and sinks.
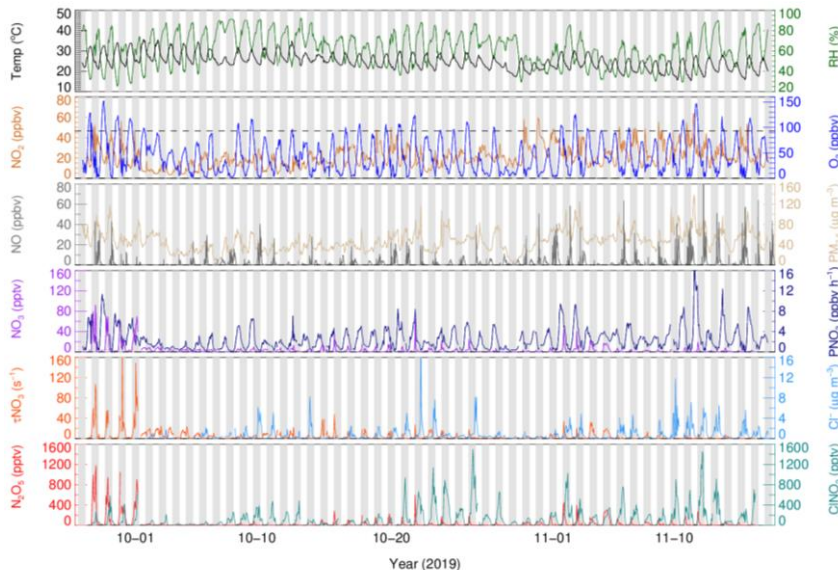
250

251 **Figure 1.** Time series of N_2O_5, $ClNO_2$ and relevant parameters. The grey dotted line in the O_3 panel
252 denotes Chinese national air quality standard for hourly maximum O_3 (200 μg m^{-3}, equivalent to 93
253 ppbv). NO_3 radical is calculated based on a thermal equilibrium with measured NO_2 and N_2O_5.

N$_2$O$_5$ existed at a moderate concentration at most nights, with the daily nocturnal peaks range from <100 pptv to 1180 pptv and nocturnal average of 64 ± 145 pptv. During the nights from 27th – 30th September, 2019, the N$_2$O$_5$ concentration was significantly higher than other nights. The NO$_3$ lifetime, calculated by steady state method (Brown et al., 2003), was much longer in the four nights than other nights, implied relative weak sink of NO$_3$-N$_2$O$_5$ for the first four nights. The lifetime of NO$_3$ was < 1 minute in general (except the first four nights), indicating active NO$_3$ chemistry at this site. The NO$_3$ concentration was calculated assuming the thermal equilibrium of NO$_2$-NO$_3$-N$_2$O$_5$, with a possible lower bias caused by the equilibrium coefficient for reversible reactions of NO$_3$ and N$_2$O$_5$ (K_{eq}) (Chen et al., 2022). Figure 1 shows the variation of calculated NO$_3$ coincided with N$_2$O$_5$. Elevated NO$_3$ occurred at the first four nights with a maximum of 90 pptv (1 h time resolution), which is comparable with the reported NO$_3$ level at other sites in Pearl River Delta (Wang and Lu, 2019; Brown et al., 2016). ClNO$_2$ showed a clear diurnal variation with high level during the night. The nocturnal average and hourly maximum were 198±232 pptv and 1497 pptv, respectively. The abundance of ClNO$_2$ and N$_2$O$_5$ are lower than those observed at the same site in 2017, with high N$_2$O$_5$ and the highest value ever observed ClNO$_2$ of 3358 pptv and 8324 pptv (1-minute time resolution), respectively (Yun et al., 2018b). ~~Which~~The difference of ClNO$_2$ level between the two campaigns conducted in 2017 and 2019 may be caused by the ~~difference of~~ aerosol loading ~~between 2017 and 2019~~. High particulate chloride ion was observed in the site with 0.74 ± 1.33 μg m^{-3} on nocturnal average, which was higher at night with a peak in the second half of night and decrease at daytime.

3. 2 Characterization of pollutants in different air masses.

We noticed the air mass is highly varied during the measurements. For example, during the period of 10/02 - 10/05, the observed ozone and ClNO$_2$ were much lower than other days; while during the period of 11/11 - 11/13, the air masses were much polluted with high O$_3$, PM$_{2.5}$ and ClNO$_2$. We therefore plotted the backward trajectories of 24 h history of air masses arriving at the measurement site at 500 m AMSL height at 00:00, 06:00, 12:00, 18:00 day by day. The measurement period was separated into three patterns meteorologically according to the analysis of backward trajectories. Table 2 listed the detailed information about the air mass classification. The air masses from northeast (and north) was the dominant with a total of 37 days, which was characterized with the outflow of the center city clusters of PRD and those from inland through long distance transport. We checked the pollutants of the air masses from PRD and the north out of PRD (e.g., Hunan or Jiangxi Province), while no significant difference was found. Therefore, we merged the two inland air masses as Type A. The second type was from the coastal or offshore from east and southeast (Type

287 B), which features the outflow of coastal cities like Shenzhen and Hong Kong, which occurred on 12

288 days in total. The third type was the clean air masses from the South China Sea (4 days, Type C).

289 Figure 2 shows three cases of each air masses mentioned above.

290 **Table 2.** The detailed information of three air mass types.

Air mass type	Periods	Days
Type A: inland air from northeast	09/26-10/01;10/08;10/11-10/20;10/24-11/10;11/14-15	37 (69.8%)
Type B: coast air from east	10/06-07; 10/09-10; 10/21-23; 11/11-13; 11/16-17	12 (22.6%)
Type C: marine air from south	10/02-05	4 (7.5%)

291 The mean diurnal profiles of measured NO_2, O_3, N_2O_5, $ClNO_2$, the particle chloride content and

292 the ratio of chloride to sodium in the three types of air masses are shown in Figure 3, with a detailed

293 summary of related parameters in nocturnal medians listed in Table 3. High levels of NO_2 and O_3

294 were observed in Type A and B air masses, with small difference of NO_2 diurnal variation during the

295 second half of night. In comparison, the two pollutants in Type C were much lower. If we focus on

296 the abundance at night, we found a large difference in NO_2 level with a sequence Type A > Type B >

297 Type C, which results in the same sequence of NO_3 productions in different air masses. The

298 nocturnal NO_2 seems to be a good indicator of the level of pollution, that nocturnal CO, $PM_{2.5}$ and

299 SO_2 also followed this order with highest concentration in Type A. These results indicate that the

300 most polluted air mass came from the inland urban regions of PRD.
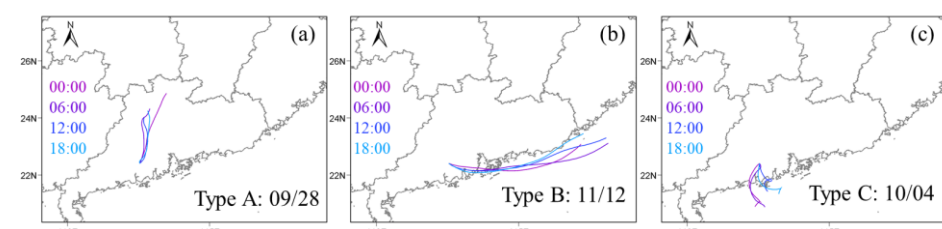
301

302 **Figure 2.** Three typical cases with air mass from different regions at 29th Sept., 12th Nov. and 4th Oct.,

303 respectively. Backward trajectory of 24 h history of air masses arriving at the measurement site with

304 500 m height at 00:00, 06:00, 12:00, 18:00.

305 Given the particulate chloride a precursor of $ClNO_2$, we examined its diurnal variations in the

306 three air mass types. The highest level of Cl^- was found in Type B, and then followed by Type A and

307 Type C (also at night). Although the diurnal profile of Cl^- in the three types is similar, the increasing

308 rate of Cl⁻ during the second half of night in Type A is much slower than those in coastal and offshore

309 air masses. This imply a difference source of chloride, which will be further discussed in the Section

310 3.4. N_2O_5 was observed with moderate concentration in the Type A air mass throughout the night,

311 with a nocturnal peak of 152.4 pptv between 20:00-21:00, while little N_2O_5 only occurred in the first

312 half of night in Type B and C with a peak of 75.9 pptv and 13.6 pptv, respectively. The concentration

313 difference may be attribute to two aspects. Firstly, the difference of $P(NO_3)$ results in more N_2O_5

314 produced in Type A. Secondly, compared with the air mass from coastal or offshore regions, the

315 nocturnal temperature and RH condition from Type A is much lower, and the loss of N_2O_5 may be

316 faster in Type B and C than that in Type A. The nocturnal median RH in Type A reached up to 67%,

317 while 78% and 79% in Type B and Type C, suggesting a favorable condition for heterogeneous

318 hydrolysis of N_2O_5 for all the three air mass types. The elevated $ClNO_2$ was observed in Type A and

319 B with a nocturnal peak of 273.6 pptv and 479.8 pptv, respectively. Significantly less $ClNO_2$ was

320 observed in Type C air mass with a peak of 82.6 pptv. The reason of the different levels of $ClNO_2$

321 observed in the three air masses types are discussed in Section. 3.4.
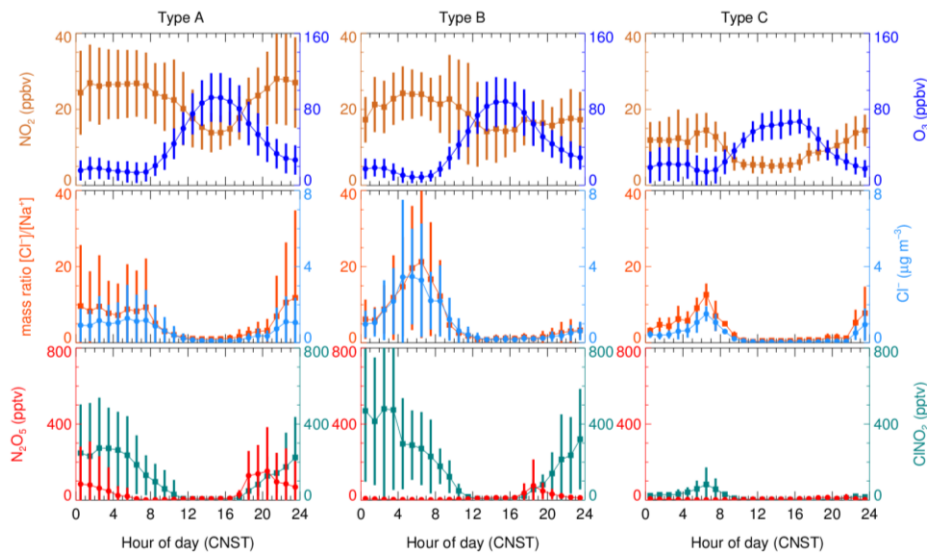
322

323 **Figure 3.** Mean diurnal profiles of N_2O_5, $ClNO_2$ and relevant parameters in the three types of air

324 masses.

325 **Table 3.** Statistics results (median ± standard deviation) of the related parameters in the three types

326 of air masses (from 18:00 to 06:00 CNST).

Air mass	Type-A	Type-B	Type-C
RH (%)	67.0 ± 11.9	78.0 ± 10.9	79.0 ± 9.1
T (°C)	22.8 ± 3.0	23.3 ± 2.2	25.6 ± 1.9
$ClNO_2$ (pptv)	131.0 ± 202.8	162.0 ± 310.1	16.7 ± 21.2
N_2O_5 (pptv)	17.8 ± 164.9	6.3 ± 64.6	2.8 ± 9.3
Cl^- ($\mu g\ m^{-3}$)	0.41 ± 1.11	0.56 ± 1.85	0.33 ± 0.51
$PM_{2.5}$ ($\mu g\ m^{-3}$)	53.0 ± 18.8	41.0 ± 21.8	32.0 ± 10.2
SO_2 (ppbv)	5.0 ± 4.7	3.4 ± 11.4	3.4 ± 4.7
Na^+ ($\mu g\ m^{-3}$)	0.12 ± 0.07	0.18 ± 0.09	0.09 ± 0.03
$P(NO_3)$ (ppbv h^{-1})	1.60 ± 1.49	1.39 ± 1.50	0.69 ± 0.49
NO_2 (ppbv)	24.8 ± 10.9	18.1 ± 6.2	11.2 ± 5.8
O_3 (ppbv)	24.4 ± 21.8	29.5 ± 23.1	22.4 ± 15.2
CO (ppbv)	540.3 ± 122.3	448.4 ± 130.7	367.5 ± 89.8

3.3 N_2O_5 uptake coefficient and $ClNO_2$ yield

In line with previous studies, we estimate N_2O_5 uptake coefficient and $ClNO_2$ yield using the measurements of N_2O_5, $ClNO_2$ and particulate nitrate (Phillips et al., 2016; Wang et al., 2018; Tham et al., 2018). By assuming both the nocturnal enhancement of nitrate and $ClNO_2$ are mainly attributed to N_2O_5 uptake processes, $ClNO_2$ yield can be solely derived by the regression analysis of $ClNO_2$ versus particulate nitrate (Wagner et al., 2012; Riedel et al., 2013). The $\varphi ClNO_2$ can then be obtained by the fitted regression slope (S, Eq. 1) and named as regression method.

$\varphi = 2S/(S+1)$ (Eq. 1)

Combining with the data of N_2O_5 and aerosol surface area, the increase in $ClNO_2$ and nitrate can be simulated simultaneously by setting the input of N_2O_5 uptake coefficient and $ClNO_2$ yield (named as simulation method). The optimal N_2O_5 uptake coefficient and $ClNO_2$ yield are obtained simultaneously by adjusting the two parameters until the simulation reproduces the observed increase $ClNO_2$ and nitrate (Phillips et al., 2016; Xia et al., 2020; Tham et al., 2018). This analysis assumes only N_2O_5 uptake process dominates the increase of $ClNO_2$ and nitrate, and other physicochemical processes like vertical transportation, depositions are less important. This method requests the air mass in the analysis duration time is relative stable and less affected by emission and transportation. In addition, it is not valid in the case with negative changes of $ClNO_2$ and nitrate. The following selection criteria is set to pick out the suitable plumes to meet the assumptions. Firstly, the consistent increase trends of $ClNO_2$ and the NO_3^- and clear correlation between them during the analysis duration should be observed with a regression coefficient threshold of 0.5, which indicates the two products have the same source. Secondary, an equivalent or faster increase of ammonium accompanied with nitrate, to ensure insignificant degas of HNO_3 to the atmosphere. The observational data were averaged to 30 min for the following analysis, the time-period of each derivation ranges from 2.5 to 10 hours. Figure 4 depicts an example of the derivation on 5th

351 November, 2019, the stable Sa indicates stable air mass during the analysis period. And the
352 prediction is well reproduced the observed increase in ClNO$_2$ and NO$_3^-$.

353   During this campaign, we carefully identified 20 plumes with clear correlations between ClNO$_2$
354 and particulate nitrate by the slope method ($R^2 \geq 0.5$). As shown in Table 4, the derived ClNO$_2$ yield
355 varied from 0.13 to 1.00 with a median of 0.45 ± 0.22 (mean value of 0.44). In the 20 plumes, we
356 derived N$_2$O$_5$ uptake coefficient and ClNO$_2$ for 12 cases in total. The results in other 8 night were not
357 valid due to the lack of Sa data (four nights) or producing unreasonably high results due to the
358 observed low N$_2$O$_5$ concentration near the detection limit biased the simulations. We show good
359 consistent of derived ClNO$_2$ yields by the two different methods. The estimated N$_2$O$_5$ uptake
360 coefficient showed a large variation and ranged from 0.0019 to 0.077 with a median of 0.0195 ±
361 0.0288 (mean value of 0.0317). The estimated γN$_2$O$_5$ is within the range determined by previous
362 field studies (Tham et al., 2018). Specifically in China, the average level of γN$_2$O$_5$ is comparable
363 with those reported in urban Beijing (Wang et al., 2017a; Wang et al., 2018), Wangdu (Tham et al.,
364 2018), and Jinan (Wang et al., 2017c) during the summertime, but systematically higher than those
365 determined in China in wintertime (Xia et al., 2021; Wang et al., 2020a; Brown et al., 2016), except
366 the case reported on the urban canopy of Beijing (Chen et al., 2020). McDuffie et al. (2018a)
367 summarized the reported φClNO$_2$ based on the observations, and we showed that the estimated
368 average φClNO$_2$ in this study is in the middle to upper end of the values reported globally (Xia et al.,
369 2021; McDuffie et al., 2018a). Due to the limited data points, we cannot distinguish the difference of
370 γN$_2$O$_5$ between the three air mass patterns. The ClNO$_2$ yields in Type A are slightly lower than those
371 in Type B with an average of 0.41 and 0.47, respectively.
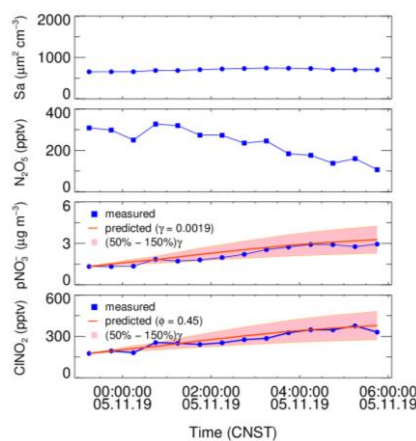
372
373 **Figure 4.** An example of the derivation of N$_2$O$_5$ uptake coefficient and ClNO$_2$ yield constrained by

374 observation of aerosol surface area, N_2O_5 and the enhancement of particulate nitrate and $ClNO_2$ on
375 5th November, 2019. The pink region presents ±50% uncertainty of N_2O_5 uptake coefficient.

Table 4. The derived N_2O_5 uptake coefficient and $ClNO_2$ yields at each night.

NO.	Period	γN_2O_5 [a]	$\varphi ClNO_2$ [a]	$\varphi ClNO_2$ [b]	r^2 [b]	Type
1	10/02 01:00-06:00	NaN	NaN	0.13	0.90	C
2	10/02 23:00-06:00	NaN	NaN	0.25	0.90	C
3	10/11 01:00-04:00	NaN	NaN	0.65	1.00	B
4	10/14 23:00-04:00	0.017	0.28	0.23	0.56	A
5	10/18 18:00-21:00	0.0059	0.42	0.40	0.90	A
6	10/20 20:30-23:00	0.045	0.44	0.47	0.71	A
7	10/21 20:30-01:00	0.061	0.52	0.54	0.90	B
8	10/22 22:30-05:00	0.066	0.58	0.61	0.62	B
9	10/24 22:00-06:00	0.065	0.26	0.23	0.74	A
10	10/25 21:00-02:00	0.077	1.00	1.00	0.92	A
11	10/28 21:00-04:00	NaN	NaN	0.15	0.74	A
12	11/01 21:00-23:30	0.022	0.35	0.32	0.83	A
13	11/02 22:00-00:30	NaN	NaN	0.29	1.00	A
14	11/03 18:00-06:00	0.0031	0.52	0.50	0.92	A
15	11/04 22:00-06:00	0.0019	0.45	0.47	0.86	A
16	11/08 00:00-06:00	0.0097	0.34	0.32	0.85	A
17	11/10 00:00-04:00	NaN	NaN	0.59	0.80	A
18	11/11 22:00-04:00	NaN	NaN	0.53	0.50	B
19	11/12 22:00-04:00	NaN	NaN	0.42	0.62	B
20	11/13 21:00-00:00	0.0070	0.70	0.75	0.92	B

377 Note: [a] the values of γN_2O_5 and $\varphi ClNO_2$ are derived by simulation method; [b] the $\varphi ClNO_2$ and the
378 correlation coefficient (R^2) between $ClNO_2$ and particulate nitrate are derived by regression method,
379 the data was filtered with a correlation coefficient obtained from linear fitting threshold of 0.5.

380 To gain insight into the factors governing the N_2O_5 uptake and $ClNO_2$ formation processes, the
381 estimated γN_2O_5 and $\varphi ClNO_2$ were compared with those predicted from complex laboratory-derived
382 and field-derived parameterizations. An aqueous inorganic iconic reaction mechanism once raised by
383 Bertram and Thornton (2009) and established a volume-limited parameterization by considering the
384 aerosol volume, surface area, nitrate content, ALWC, and chloride content (named BT09, Eq. 8).

385 $$\gamma_{BT09} = \frac{4H_{aq}Vk}{CS_a}\left(1 - \frac{1}{1 + \frac{k_3[H_2O]}{k_{2b}[NO_3^-]} + \frac{k_4[Cl^-]}{k_{2b}[NO_3^-]}}\right) \qquad (8)$$

386 Where H_{aq} is Henry's law coefficient of N_2O_5, V is the aerosol volume; k is equal to1.15×10^6-(1.15

387    $\times 10^6)^{\exp(-0.13[H2O])}$; k_3/k_{2b} is the ratio of reaction rate of H_2O versus NO_3^- to $H_2ONO_2^+$ that was set to

388   0.06, and k_4/k_{2b} is the ratio of reaction rate of Cl^- versus NO_3^- to $H_2ONO_2^+$ that was set to 29

389   (Bertram and Thornton, 2009). The mean values of particulate volume to surface ratio (V/Sa) was

390   measured. A simple parameterization (EJ05) considered the effect of enhanced RH and temperature

391   on N_2O_5 uptake was also included (Evans and Jacob, 2005). In addition, the recently established

392   empirical parameterization based on the same framework (Eq. 8, named Yu20), optimized some

393   parameters according to the meta-analysis of five field measurements in China by Yu et al. (2020),

394   also assessed in the study. Figure 5(a) shows the correlation of estimated γN_2O_5 versus the

395   parameterization. All the three parameterizations fail to predict the high values. The simple

396   parameterization of EJ05 had the best performance with a high correlation and a consistent

397   prediction of the median value. While other two parameterizations, BT09 and Yu20, underestimated

398   the observed γN_2O_5. Figure 6(a-h) show the dependence of the observed γN_2O_5 on the factors

399   reported in previous literatures that possibly alert the processes of N_2O_5 uptake and $ClNO_2$ formation.

400   We show that γN_2O_5 highly correlated with the ambient RH as well as liquid water content,

401   confirming the critical role of water content in N_2O_5 uptake and explained the reason why EJ05 had a

402   good performance. The dependence of γN_2O_5 on nitrate mass concentration does not follows the rule

403   of nitrate suppressing effect (Wahner et al., 1998), which may be due to the covariance of nitrate and

404   liquid water content. With respect to other factors, insignificant impacts on the N_2O_5 uptake are

405   obtained.

406
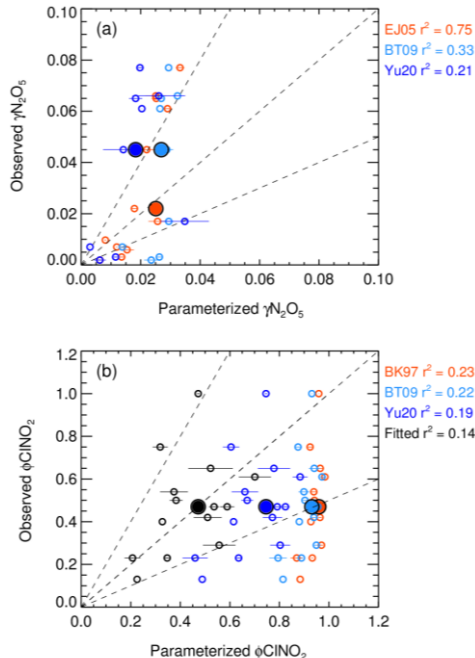
Figure 5. The inter-comparison of observation and parameterization of N_2O_5 uptake coefficient (a)
and $ClNO_2$ yield (b). The larger size of solid dots represents the median results. The parametrizations
of EJ05, BT09, Yu20 and BK97 cited from Evans and Jacob (2005), Bertram and Thornton (2009),
Yu et al. (2020), Behnke et al. (1997), respectively. The fitted $ClNO_2$ yield (colored by black) in
panel (b) shows the best fitting result in the study by adopting the k_4/k_3 of 32.0.

Bertram and Thornton (2009) also proposed a $ClNO_2$ yield parameterization method that
considering the ratio of ALWC and chloride content (Eq. 9), here the k_4/k_3 was the ratio of reaction
rate of $H_2ONO_2^+$ versus Cl^- to H_2O and adopted as 483 ± 175. Behnke et al. (1997) determined this
ratio of 836 ± 32, while it is estimated to be 105 ± 37 in Yu et al. (2020).

$$\varphi_{BT09} = \left(\frac{[H_2O]}{1+k_4/k_3[Cl^-]}\right)^{-1} \tag{9}$$

Figure 5(b) shows that all the predicting $ClNO_2$ yield based on the abovementioned
parameterizations overestimated the observations. The performance of the parameterization schemes
of BK97 and BT09 based on the model aerosol conditions with an overestimation up to ~100% are
expected and consistent with previous studies, which may be caused by the unaccounted potentially
competitive effect of other species like organics, sulfate for the $NO_2^\pm$ intermediate (McDuffie et al.,

设置了格式: 上标

422 2018a; Staudt et al., 2019; Xia et al., 2021; Wang et al., 2017d). Although the empirical

423 parameterization (Yu20) based on field observations improved the prediction and narrowed the gap

424 effectively, the overestimation is still large with an average of ~50%, which indicated that the yield

425 are more strongly suppressed in this study than those observed in the campaigns of Yu et al. (2020).

426 The factor 32.0 (k_4/k_3 in Eq. 9) was derived by iterative algorithms to achieve the best consistent

427 between the observed and parameterized $ClNO_2$ yield, which is smaller than the Yu20 parameters by

428 factors of 3.3. We examined the relationships of $ClNO_2$ yields with aerosol water content and other

429 aerosol compositions as shown in Figure 6(i-p). We show that $\varphi ClNO_2$ only weakly correlated with

430 the content of chloride (including the mass ratio and fraction in $PM_{2.5}$) and the molar ratio of chloride

431 to water, confirmed the dependence found in laboratory studies. However, we did not find the

432 dependence of the yields with aerosol organic or sulfate, as well as the RH and water alone in the

433 campaign, implying the $ClNO_2$ yield mechanism is much more complicated than the laboratory

434 conditions.

435
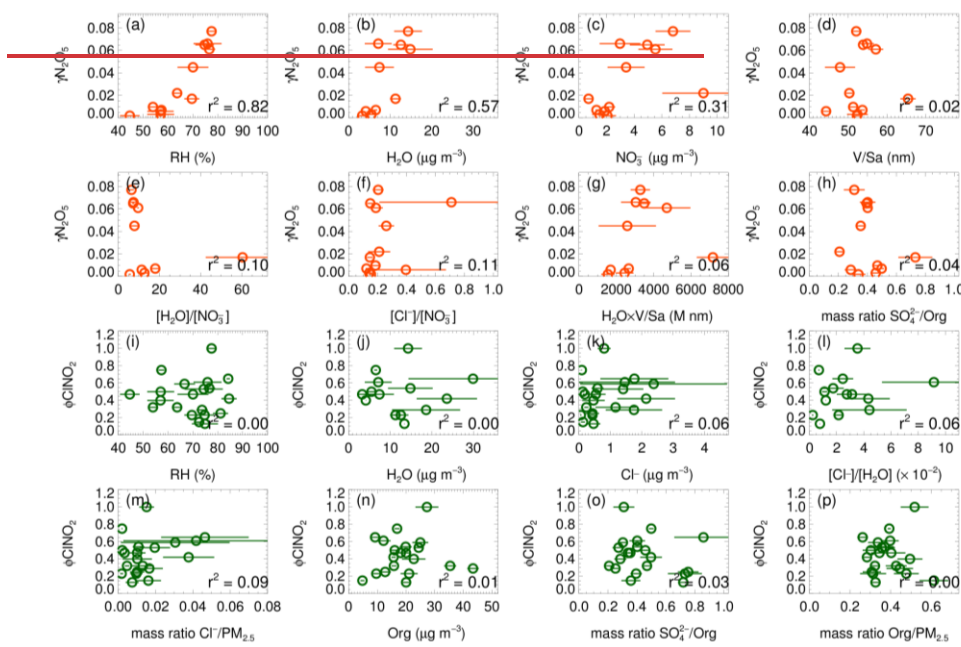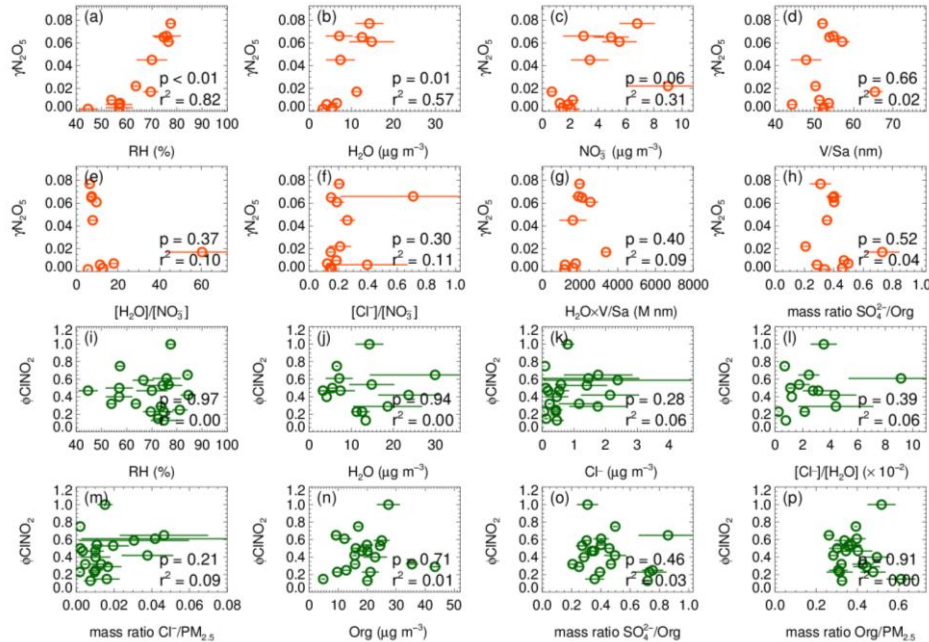
Figure 6. The estimated N_2O_5 uptake coefficient and $ClNO_2$ yield versus related parameters.

3.4 The factors influence $ClNO_2$ formation

The $ClNO_2$ formation can be largely affected by the budget of NO_3-N_2O_5 and N_2O_5 uptake processes. The variation of NO_3 loss by VOC and NO alert the NO_3 loss distribution by N_2O_5 uptake and $ClNO_2$ formation indirectly. Figure 7 shows the correlation between daily median $ClNO_2$ and mass concentration of chloride, $PM_{2.5}$ and NO_3 production rate for the three types of air masses. Due to the limited dataset of type C, the correlation analysis may not make sense, therefore, we did not take type C into consideration in detailed discussion. We show that the mass concentration of chloride also showed a correlation coefficient with $ClNO_2$ by 0.66 and 0.31 for type A and B, respectively. Furthermore, the mass concentration of $PM_{2.5}$ correlated reasonably with the $ClNO_2$ formation with the correlation coefficient of 0.39 and 0.62 for type A and B, respectively. But, the levels of $ClNO_2$ demonstrate little relationship with the nitrate production rate. This is quite different from the results observed in United Kingdom, where the $ClNO_2$ levels are mainly controlled by NO_2 and O_3, rather than by the N_2O_5 uptake processes (Sommariva et al., 2018).
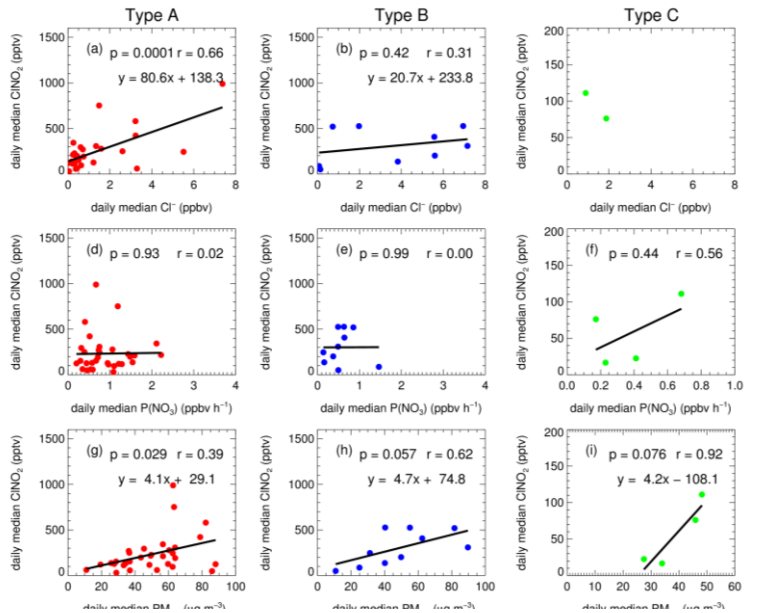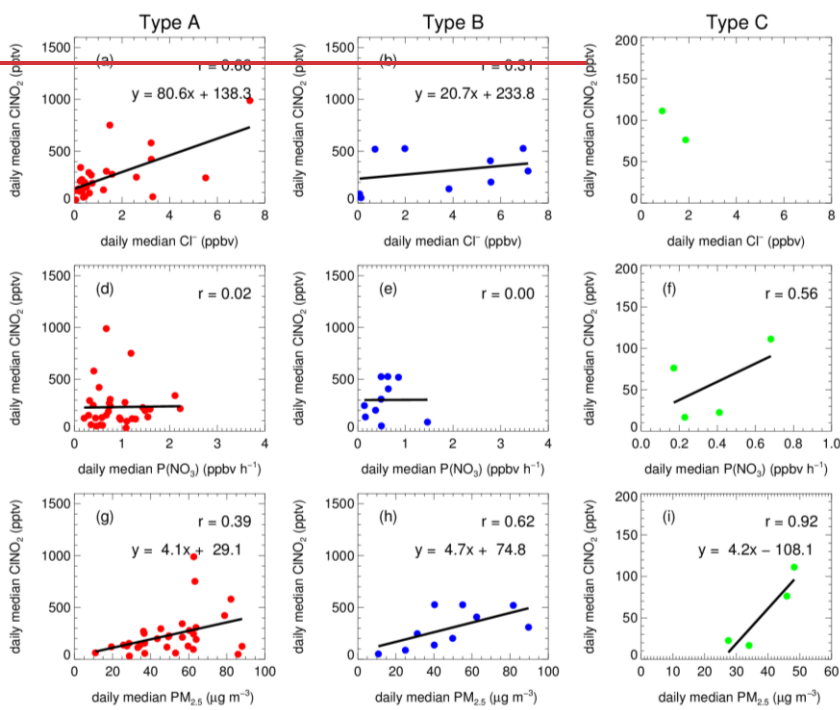
Figure 7. The functional dependence of daily median of $ClNO_2$ on particulate chloride, nitrate radical production rate and $PM_{2.5}$ in the air mass of Type A (a, d, g), Type B (b, e, h) and Type C (c, f, i).

The low correlation between $ClNO_2$ and NO_3 production rate is within expectations. In general, the production of nitrate radical controls the total budget of N_2O_5, if N_2O_5 uptake dominated the sink of NO_3, as the result the N_2O_5 uptake and its products would show good correlation with NO_3 production rate. But in fact, NO_3 loss can also be affected by other loss pathways, like the reactions with NO and VOCs. In many cases, the NO_3 loss is dominated by VOC or NO, that means the $ClNO_2$ formation is suppressed. If the two loss pathways are highly varied due to irregular emissions, then the relationship between $ClNO_2$ and NO_3 production rate would be less correlated. We confirmed large variations of NO and VOC (not shown) in hourly and daily scales, which means the proportion of N_2O_5 uptake to the total loss of NO_3 is highly varied correspondingly. In addition, the variation of N_2O_5 uptake coefficient and $ClNO_2$ yield also result in the weak correlation between NO_3 production rate and $ClNO_2$ concentration. The weak correlation reflects the highly variable chemical processes from NO_3 production to $ClNO_2$ production in this region. ~~Overall, the low correlation in the study indicated that the $ClNO_2$ formation through N_2O_5 uptake is not limited by NO_3 formation processes, at least in Type A and B. With respect to the air mass Type C, $ClNO_2$ showed correlation with $P(NO_3)$ with the correlation coefficient of 0.56.~~

As the precursor of $ClNO_2$, higher concentrations of particulate chloride result in high $ClNO_2$ yield from N_2O_5 uptake to some extent, as evidenced by our field observation (Figure 6) and previous laboratory studies (Bertram and Thornton, 2009; Roberts et al., 2009; Ryder et al., 2015). High $PM_{2.5}$ concentrations usually provide more aerosol surface area to promote N_2O_5 uptake. The close relationship between $ClNO_2$ and $PM_{2.5}$ indicate that aerosol surface area, most likely, is a critical factor that limited $ClNO_2$ formation. The proportion of nitrate in the total $PM_{1.0}$ was small with an average of 10.4%, therefore the correlation of $ClNO_2$ and $PM_{2.5}$ cannot attribute to the covariance between nitrate and $PM_{2.5}$. In addition, the $ClNO_2$ level in the air mass of Type B show higher correlation to both Cl^- and $PM_{2.5}$ than type A, suggesting that the $ClNO_2$ formation in Type B is more effectively affected by the levels of chloride and $PM_{2.5}$.

Recently model simulation indicated that the $ClNO_2$ chemistry level is sensitive to the emission of chloride in PRD (Li et al., 2021). In this study, a question raised that where is the source of chloride? The mass ratio of Cl^-/Na^+ is often used as an indicator of sea salt or anthropogenic sources to chloride with a threshold of 1.81 (Yang et al., 2018; Wang et al., 2016). High ratio means the particulate chloride affected by anthropogenic emission rather than sea salt. We determine that the

mean mass ratios of Cl⁻ to Na^+ are 5.3, 6.3 and 3.1 in Type A, B and C, respectively (Figure 3). This indicated that $PM_{2.5}$ sampled during the campaign was not strongly influenced by fresh sea salt aerosols. In the three types, the Type C air mass had a lowest ratio and may be influenced by both sea salt and anthropogenic emissions, which seems reasonable since it come from South China Sea. If we assume that Type A air mass is free of sea salt and only influenced by anthropogenic activities, the higher ratio implies more intensive chloride source in Type B. The correlation between particulate chloride and some possible indicators, including K^+, benzene, SO_2, CO, acetonitrile (CH_3CN), were examined day by day. Figure 8 shows the max correlation coefficient (R^2) in each day with a threshold of 0.5. We filtered out 39 out of 46 days during this campaign with a fraction of 85%. Among the 39 days, a total of 11 days is associated with strongest correlation between Cl⁻ and benzene, which is typically come from industrial emissions. Cl⁻ also correlated with K^+, CO and CH_3CN in 19 day in total, implies potential contributions from biomass burning emissions. In total of 9 days for highest correlations of Cl⁻ with SO_2 indicated coal-fired power plants emissions may also contributed to Cl⁻ emission. We summarized that the source of chloride may be highly varied from different anthropogenic activities including biomass burning, industrial processes as well as coal-fired power plants. The statistic results in Table 5 suggest that the Cl⁻ in air mass of Type A were affected by various sources, especially related to the sources associated with K^+, benzene and CH_3CN; the Cl⁻ in Type B was mainly contributed by the similar source of CO, and Type C was only affected by coal-fired power plants emissions. In addition, Figure 8 showed that there are 2 days that the correlations between Cl⁻ and Na^+ exceeded the max of the selected anthropogenic factor matrix, indicated that the aerosol still also impacted by sea salt to some extent.
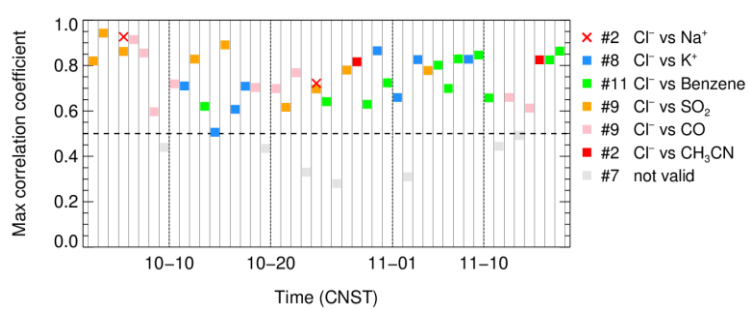
Figure 8. The max correlation coefficient between particulate chloride and a selected parameter matrix (including K^+, benzene, SO_2, CO, acetonitrile (CH_3CN)) in each day. The labelled number in each legend indicates the days be the maximum, the dashed line denotes the threshold of 0.5 (39 valid days out of 46 in total). The cross means the correlation coefficient between Cl⁻ and Na^+ is

512 larger than the max.

513 **Table 5.** The statistic of the days for highest factors correlated with particulate chloride in different
514 air mass pattern.

~~factors~~Factors	Type A	Type B	Type C
K^+	8	0	0
Benzene	9	2	0
SO_2	5	1	3
CO	4	5	0
CH_3CN	2	0	0

515 **3.5 The impacts of $ClNO_2$ on atmospheric oxidation**

516 In this section, we focus on the assessment of the impact of $ClNO_2$ photolysis on the source of
517 radicals and the contribution to the atmospheric oxidation. Figure 9 shows the diurnal accumulation
518 of ROx production rate from model simulations with $ClNO_2$ chemistry in the three types of air mass.
519 The total ROx production rate was higher in Type A and then followed by Type B and C, in which
520 photolysis of HONO, HCHO, O_3 and OVOCs had large contributions. In addition, we noticed that
521 the significant role of OVOCs (including photolysis and reacts with O_3) in producing ROx at this site,
522 especially in the Type A and B air mass. This result is consistent with that constrained by observed
523 OVOCs in Guangzhou City (Wang et al., 2022c).
524 Cl radical, liberated by $ClNO_2$, enhanced little ROx production, with a morning peak contribution of
525 1.3%, 2.2% and 1.8% for Type A, B, C, respectively (08:00-09:00). The contribution of $ClNO_2$
526 photolysis to the production of ROx is less than 1% on daytime average~~d~~, similar to the results
527 obtained in winter Shanghai (Lou et al., 2022) as well as North China (Xia et al., 2021), and much
528 lower compared to previous studies reported in summer time in ~~in both north and south~~ China (Tan
529 et al., 2017; Tham et al., 2016). However, another winter campaign conducted in Hongkong in winter
530 showed much more significant impacts compared with our observation(Wang et al., 2016), indicated
531 that the $ClNO_2$ chemistry can also had a large influence on the radical formation in wintertime.
532 ~~(Tham et al., 2016;Wang et al., 2016)In addition, we noticed that the significant role of OVOCs~~
533 ~~(including photolysis and reacts with O₃) in producing ROx at this site, especially in the Type A and~~
534 ~~B air mass. This result is consistent with that constrained by observed OVOCs in Guangzhou City~~
535 ~~(Wang et al., 2022c).~~
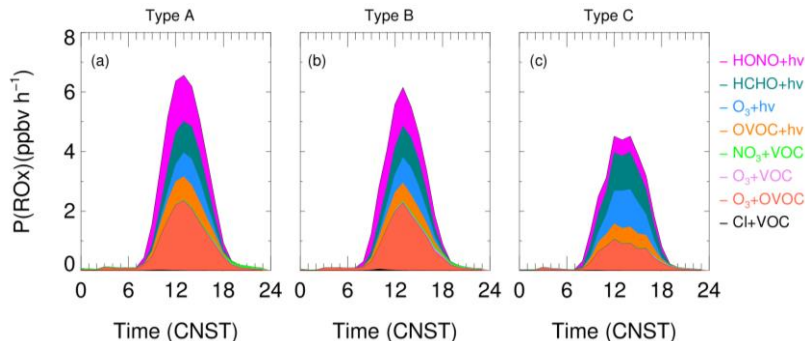
536
537 **Figure 9.** The diurnal cycle and distribution of ROx production rate in the three types air masses.

538   Figure 10 shows the enhancement of OH, HO$_2$ and RO$_2$ radicals with the consideration of ClNO$_2$
539 chemistry. The enhancement of the three radicals peaked in the morning. On average, OH
540 concentration was enhanced by 1.5% to 2.6% in different air masses. The percentage of enhancement
541 for HO$_2$ radical was 1.9% to 4.6%, whereas the enhancement for RO$_2$ was a little bit higher (3.0% to
542 6.8%). In general, the enhancement of radicals was more significant in Type B than other two types
543 of air masses, which is related to elevated ClNO$_2$ concentrations for these air masses. Low ClNO$_2$
544 and other radical precursors led to an earlier enhancement peak (08:00-09:00) in Type C and lasted a
545 short time period. Although the increase peak occurred later at 09:00-10:00 for the air mass of Type
546 A and Type B, the increase lasted for a longer time and had a longer effect. Overall, daytime OH,
547 HO$_2$ and RO$_2$ enhanced by 1.0%, 2.0%, and 3.0% on campaign average.
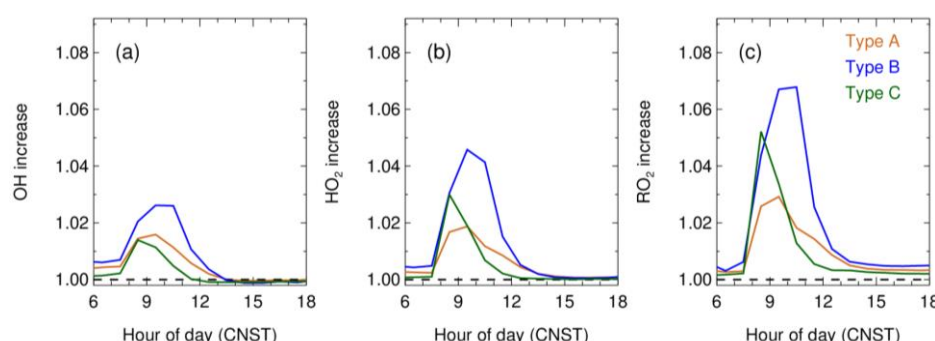
548
549 **Figure 10.** The diurnal cycle on the enhancement of OH (a), HO$_2$ (b), RO$_2$ (c) by ClNO$_2$ chemistry
550 in the three air mass patterns.

551   Figure 11 depicts the integral enhancement of O$_3$ production by ClNO$_2$ photolysis varied from less

than 0.1 ppb to 4 ppb day by day, with a percentage of <1% to 4.9% with a median of 0.8%. Our results are comparable with the winter case in North China (Xia et al., 2021). The next day O_3 enhancement was highly correlated with the level of $ClNO_2$ with the correlation coefficient of 0.7 (Fig. 11(a)). The daily net O_3 production enhanced by 0.70 ppbv h⁻¹ (0.9%), 1.02 ppbv h⁻¹ (1.9%), 0.24 ppbv h⁻¹ (0.6%) on daytime accumulation in Type A, B, C, respectively, which is consistent with the nocturnal level of $ClNO_2$ in the three air masses presented in Table 3.
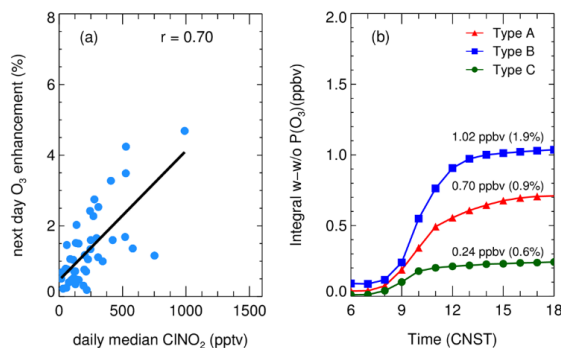
Figure 11. (a) The correlation of daily median $ClNO_2$ (18:00-06:00) and its impact on next day net O_3 production enhancement during the campaign; (b) the average contribution of daytime integral O_3 by $ClNO_2$ mechanism in the three types of air masses.

Table 6 summarized the observation-constrained box model simulation results about the impacts of $ClNO_2$ chemistry. The average $ClNO_2$ concentration in the observation is moderate compared with previous observations, other radical precursors (e.g., HCHO) also elevated at the same time. This leads to a large total radical and ozone production rate and relative minor contribution by $ClNO_2$ chemistry. Which indicates that the contribution of $ClNO_2$ chemistry is affected by the budget of other radical precursors. In addition, significant contribution by $ClNO_2$ chemistry to photochemical pollution also frequently observed in different campaigns (Tham et al., 2016; Wang et al., 2016), in which the receptor site may have aging plumes with higher $ClNO_2$ and thus larger contributions (Wang et al., 2016), suggests the large variability of $ClNO_2$ and its environmental impacts at various air masses. Here, our observations should be representative of the local condition and reflects the chemistry and impacts of $ClNO_2$ on the air pollutions in PRD region.

Table 6. The summary of impacts of $ClNO_2$ on the next-day enhancement of ozone and radical production based on box model that constrained by field observations in previous literatures.

Location	Duration	ClNO₂ peak (ppb)	Daytime average Enhancement P(O₃)	Daytime average Enhancement P(RO₃)	References
Heshan, CN	2019. 11	1.5	1.0%-4.9%	<2.2%	this work
Shanghai, CN	2020.10-11	0.4	-	<1.0%	Lou et al., 2022
Wangdu/Beijing/ Mt. Tai, CN	2017-2018	1.7	1.3%-6.2%	1.3%-3.8%	Xia et al., 2021
Wangdu, CN	2014.6-7	2.1	3.0%	<10.0%	Tham et al., 2016
Seoul, Korea	2016.5-6	2.5	1.0-2.0%	-	Jeong et al., 2019
Hongkong, CN	2013.11-12	4.7	11.0-41.0%[a]	-	Wang et al., 2016
California, US	2010.5-6	1.5	15.0%[b]	17.0%	Riedel et al., 2014

Note: [a] used box model to estimate the following evolution after the plume passing measurement site and the impacts on the next day air quality; [b] not constrained the observed ClNO₂ concentration but simulated the observed maximum ClNO₂ case (1.5 ppbv ClNO₂) to predict the corresponding upper contribution.

Previous studies suggest that chlorine radicals from ClNO₂ photolysis may contribute significantly to the oxidation of some VOCs species, especially for long-chain alkanes(Shi et al., 2020; Wang et al., 2022b). The oxidation of long-chain alkanes (C10~14 n-alkanes) by ~~chloride~~ chlorine and OH radicals during the morning hour (~~08~~09:00 — ~~09~~10:00) were also evaluated based on modeled oxidants concentration. We observe small contributions of chlorine radical with a percentage of 4.3%, 4.3% and 3.8% for n-decane, n-dodecane, and n-tetradecane, respectively, during the period (Oct. 16th to Nov. 17th, 2019) when the long-chain alkanes measurement was valid. We also checked the role of chlorine radicals in short-chain alkanes oxidation, obtaining a slightly larger contribution than the long-chain alkanes, which is attributed to a relatively larger reaction rate constants between Cl with OH with respect to the short-chain alkanes. The daytime average contributions of Cl ranged from 1.4% - 1.6% varied by the chain length of the alkanes. Therefore, we concluded that chlorine radicals liberated by ClNO₂ photolysis play a role in the oxidation of alkanes in the morning time, but are not critical compared with OH oxidation on the daytime average. We note that several studies reported other sources produced a large number of halogen radicals like Cl₂ (Liu et al., 2017; Xia et al., 2020), BrCl (Peng et al., 2021), the daytime reaction of HCl with OH (Riedel et al., 2012; Eger et al., 2019; Li et al., 2019). These may cause more alkanes oxidized by halogen radicals. However, it is not possible to assess the overall impacts by constraining all precursors of chlorine radical in this work, which may warrant further investigation by more comprehensive field studies equipped with the instruments for detecting these species.

We observe small contributions of chloride radicalchlorine radical with a percentage of 3.2%, 3.7% and 4.2% for n-decane, n-dodecane and n-tetradecane, respectively. The contributions reduced to <1% on daytime average. We also checked the role of chloride chlorine radicals in short chain alkanes oxidation, obtaining an even smaller contribution than the long-chain alkanes. The contributions reduced to <1% on daytime average. Therefore, we concluded that, chloride radicalchlorine radicals liberated by ClNO$_2$ photolysis, is not critical to the oxidation of alkanes compared with OH oxidation during the campaign. We note that several studies reported other sources produced large amount of chloride radical halogen radicals like Cl$_2$ (Liu et al., 2017; Xia et al., 2020), BrCl (Peng et al., 2021), the daytime reaction of HCl with OH (Riedel et al., 2012; Eger et al., 2019; Li et al., 2019), Br$_2$ (Xia et al., 2022). However, it is not possible to assess the overall impacts by constraining all precursors of chloride radicalchlorine radical in this work, which may warrant further investigation by more comprehensive field studies equipped with the instruments for detecting these species.

4. Conclusion

An intensive field study in Pearl River Delta took place during a photochemical pollution season from Sept. 26th to Nov. 17th, 2019, providing a comprehensive observation dataset to understand the ClNO$_2$ chemistry and its impacts on the air quality. In general, wWe observed a wide variation for determining factors of ClNO$_2$ formation in different kinds of air masses. We found that the air masses highly varied from different regions and divided in three types according to the results of backward trajectory. Two of them,types of air mass from northern and northeastern inland cities and the eastern coastal regions, features polluted with elevated O$_3$ and related trace gases like NOx and CO. Correlation analysis showed that ClNO$_2$ formation is limited by chloride availability and PM$_{2.5}$ concentrations (mostly due to aerosol surface area) at this site. In general, we observed a wide variation for determining factors of ClNO$_2$ formation in different kinds of air masses.

We estimated the N$_2$O$_5$ uptake coefficients and ClNO$_2$ yield during this campaign and assessed the performance of previous parameterizations schemes. The newly developed observation-based empirical parameterization was also checked and showed an overall underestimation. We showed the γN$_2$O$_5$ only strongly correlated with RH, and the parameterization proposed by Evans and Jacob (2005) showed a considerable consistent with the observation. The ClNO$_2$ yield only showed weak correlation with the content of particle chloride, and the exist parameterizations systematically overestimated the yield.

The particulate chloride mainly originated from anthropogenic emissions rather than sea salt. However, the specific contributing source of chloride in this region cannot be determined, due to the varying correlation relationship with different kinds of anthropogenic emission indicators day by day.

批注 [81]:

设置了格式: 上标
设置了格式: 上标

~~We can only infer that the air mass of Type A affected by most complicated anthropogenic emissions including biomass burning, coal-fired power plants as well as the even possible usage of industrial solvents.~~ This result highlights the $ClNO_2$ chemistry may be triggered by many kinds of anthropogenic activities in the PRD regions (Wang et al., 2016; Yang et al., 2018). ~~The sources of particulate chloride warrant further detailed exploration using the dataset along with other observations in this region.~~

~~In the end, we investigate the impacts of $ClNO_2$ chemistry on atmospheric oxidation by a box model. It is demonstrated that~~Observation-constrained box model revealed ~~chloride radical~~chlorine radicals liberated by $ClNO_2$ chemistry had a relatively small contribution to the following daytime level of ~~OH, HO_2, and RO_2~~RO_x radicals ~~, as well as a small enhancement of~~and O_3 ~~and ROx production in all the three types of air masses~~in this region. ~~The impacts of $ClNO_2$ chemistry were larger in the Type B than that of Type A. Overall, t~~The small contribution of $ClNO_2$ chemistry in PRD region may be due to the limited $ClNO_2$ produced by N_2O_5 uptake processes, and other strong primary sources of radicals weakened its contribution indirectly. Given complex source of particulate chloride, we call for more field investigations to address the ~~chloride chemistry~~chlorine chemistry and its roles in air pollutions in China.

设置了格式： 字体：倾斜，下标

Data availability. The datasets used in this study are available from the corresponding author upon request (byuan@jnu.edu.cn).

Author contributions. H.C.W. and B.Y. designed the study. E.Z, X.X.Z. and H.C.W. operated and calibrated the CIMS, H.C.W. analyzed the data, H.C.W. and B.Y. wrote the manuscript with inputs from all coauthors.

Competing interests. The authors declare that they have no conflicts of interest.

Acknowledgements. This work was supported by the National Natural Science Foundation of China (grant No. 41877302, 42175111, 42121004), Guangdong Natural Science Funds for Distinguished Young Scholar (grant No. 2018B030306037), Key-Area Research and Development Program of Guangdong Province (grant No. 2019B110206001), and Guangdong Innovative and Entrepreneurial Research Team Program (grant No. 2016ZT06N263). This work was also supported by Special Fund Project for Science and Technology Innovation Strategy of Guangdong Province (Grant No.2019B121205004). The authors gratefully acknowledge the Jinan University science team for

662 their technical support and discussions during this campaign. We thank for the NOAA Air Resources

663 Laboratory for providing the HYSPLIT model.

664 **Appendix**

665 **A1. The measurement background and calibration of CIMS**

666 The background measurement of $ClNO_2$ and N_2O_5 was performed during the campaign. Figure 1A

667 showed an example of the background check at the beginning of the campaign, which confirmed the

668 negligible background signal in the measurement of $ClNO_2$ and N_2O_5 in the ambient condition. The

669 calibration of $ClNO_2$ measurement sensitivity has been introduced in Wang et al. (2022a). In brief, a

670 nitrogen flow (6 mL min^{-1}) containing 10 ppmv Cl_2 was passed over a slurry containing $NaNO_2$ and

671 NaCl to produce $ClNO_2$ (Thaler et al., 2011), and NaCl was included in the slurry in order to

672 minimize the formation of NO_2 as a byproduct. The mixed flow containing $ClNO_2$ was then

673 conditioned to a given RH and sampled into the CIMS instrument. To quantify $ClNO_2$, the mixed

674 flow was delivered directly into a cavity attenuated phase shift spectroscopy instrument (CAPS,

675 Model N500, Teledyne API) to measure background NO_2 concentrations or through a thermal

676 dissociation tube at 365 ºC to fully decompose $ClNO_2$ to NO_2, and the total NO_2 concentrations were

677 then determined using CAPS. The differences in the measured NO_2 concentrations with and without

678 thermal dissociation was equivalent to $ClNO_2$ concentrations. The CAPS instrument had a detection

679 limit of 0.2 ppbv in 1 min for NO_2 and an uncertainty of ~10%. To calibrate CIMS measurements of

680 N_2O_5, a humidity adjustable mixed flow containing stable N_2O_5, which was produced via O_3

681 oxidation of NO_2, was sampled into the CIMS instrument to obtain a normalized humidity

682 dependence curve of N_2O_5. While the concentration of N_2O_5 source is not quantified due to the

683 absence of a N_2O_5 detector, so we delivered the N_2O_5 source flow through a supersaturated sodium

684 chloride solution to convert N_2O_5 to $ClNO_2$ with a unit efficiency at 50% RH, which is a widely used

685 method for the calibration of $ClNO_2$ by CIMS technique. The absolute N_2O_5 sensitivity at ~~RH~~ 50%

686 RH can be realized and then scaled to other humidity condition by the normalized N_2O_5 sensitivity

687 curve determined before. The sensitivity curves for N_2O_5 and $ClNO_2$ to water content were shown in

688 Figure ~~A1~~A2. In this study, the sensitivity of the instrument was calibrated after the campaign. The

689 main parameters (pressure: voltages, etc.) of the CIMS were checked every day and were relatively

stable, indicating that the CIMS is operating stably during the campaign.

Figure ~~A2~~ A3 shows the high-resolution peak fitting results of typical mass spectra at m/z 235 and m/z 208 for N_2O_5 and $ClNO_2$ in three air mass patterns, respectively. The peaks of N_2O_5 and $ClNO_2$ were clearly resolved in the mass spectra. The peak of $IN_2O_5^-$ can be well retrieved by separating a large adjacent peak of $C_2H_4IO_3S^-$ in the air masses affected by marine emissions (Type B and C), which might be hydroperoxymethyl thioformate (HPMTF) from dimethyl sulfide oxidation (Veres et al., 2020). The interference signals including $H_3INO_2S^-$ for $ClNO_2$ measurements can also be well separated in all the three air mass patterns. These results underline the necessity and feasibility in the application of ToF analyzer in detecting N_2O_5 and $ClNO_2$ with iodide CIMS.
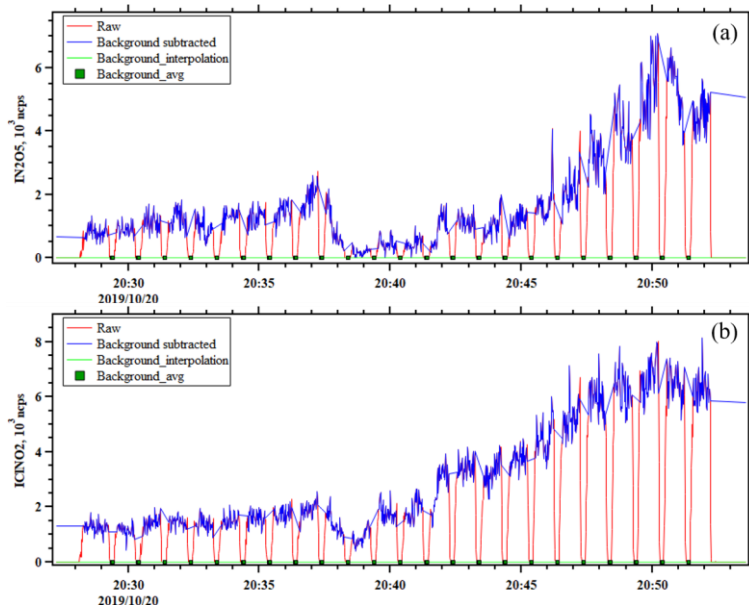
Figure A1. An example of background measurement for N_2O_5 (a) and $ClNO_2$ (b) in October 20th, 2019.

703

704
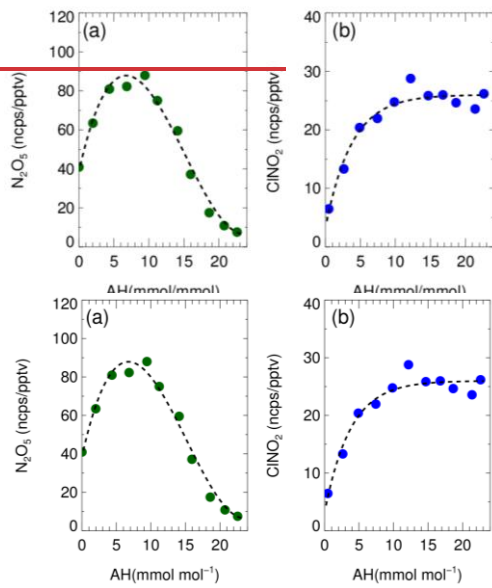
705 **Figure ~~A1~~A2.** CIMS sensitivities as a function of absolute ~~water concentration~~humidity (AH) for (a)

706 N_2O_5 and (b) $ClNO_2$.

707
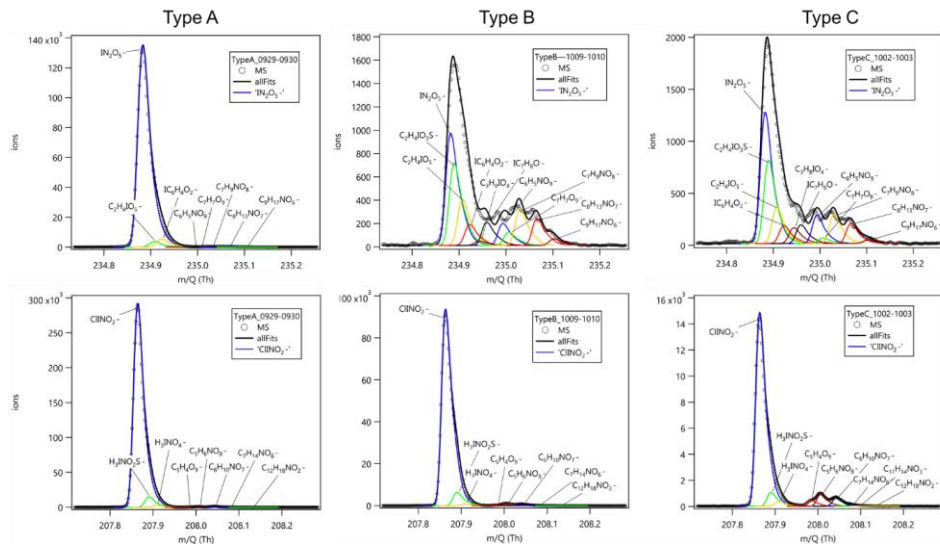
708 **Figure ~~A2~~A3.** Cases of high-resolution spectra fitting for N_2O_5 and $ClNO_2$ by ToF-CIMS under

709 three air mass patterns.

710

Reference

Anttila, T., Kiendler-Scharr, A., Tillmann, R., and Mentel, T. F.: On the reactive uptake of gaseous compounds by organic-coated aqueous aerosols: Theoretical analysis and application to the heterogeneous hydrolysis of N2O5, J Phys Chem A, 110, 10435-10443, Doi 10.1021/Jp062403c, 2006.

Atkinson, R., and Arey, J.: Atmospheric degradation of volatile organic compounds, Chem Rev, 103, 4605-4638, 10.1021/cr0206420, 2003.

Atkinson, R., Baulch, D. L., Cox, R. A., Crowley, J. N., Hampson, R. F., Hynes, R. G., Jenkin, M. E., Rossi, M. J., and Troe, J.: Evaluated kinetic and photochemical data for atmospheric chemistry: Volume II - gas phase reactions of organic species, Atmospheric Chemistry and Physics, 6, 3625-4055, DOI 10.5194/acp-6-3625-2006, 2006.

Bannan, T. J., Booth, A. M., Bacak, A., Muller, J. B. A., Leather, K. E., Le Breton, M., Jones, B., Young, D., Coe, H., Allan, J., Visser, S., Slowik, J. G., Furger, M., Prevot, A. S. H., Lee, J., Dunmore, R. E., Hopkins, J. R., Hamilton, J. F., Lewis, A. C., Whalley, L. K., Sharp, T., Stone, D., Heard, D. E., Fleming, Z. L., Leigh, R., Shallcross, D. E., and Percival, C. J.: The first UK measurements of nitryl chloride using a chemical ionization mass spectrometer in central London in the summer of 2012, and an investigation of the role of Cl atom oxidation, Journal of Geophysical Research-Atmospheres, 120, 5638-5657, 10.1002/2014jd022629, 2015.

Bannan, T. J., Bacak, A., Le Breton, M., Flynn, M., Ouyang, B., McLeod, M., Jones, R., Malkin, T. L., Whalley, L. K., Heard, D. E., Bandy, B., Khan, M. A. H., Shallcross, D. E., and Percival, C. J.: Ground and Airborne UK Measurements of Nitryl Chloride: An Investigation of the Role of Cl Atom Oxidation at Weybourne Atmospheric Observatory, Journal of Geophysical Research-Atmospheres, 122, 11154-11165, 10.1002/2017jd026624, 2017.

Bannan, T. J., Khan, M. A. H., Le Breton, M., Priestley, M., Worrall, S. D., Bacak, A., Marsden, N. A., Lowe, D., Pitt, J., Shallcross, D. E., and Percival, C. J.: A Large Source of Atomic Chlorine From ClNO2 Photolysis at a UK Landfill Site, Geophysical Research Letters, 46, 8508-8516, 10.1029/2019gl083764, 2019.

Behnke, W., George, C., Scheer, V., and Zetzsch, C.: Production and decay of ClNO2, from the reaction of gaseous N2O5 with NaCl solution: Bulk and aerosol experiments, Journal of Geophysical Research-Atmospheres, 102, 3795-3804, Doi 10.1029/96jd03057, 1997.

Bertram, T. H., and Thornton, J. A.: Toward a general parameterization of N2O5 reactivity on aqueous particles: the competing effects of particle liquid water, nitrate and chloride, Atmospheric Chemistry and Physics, 9, 8351-8363, 2009.

Bohn, B., Corlett, G. K., Gillmann, M., Sanghavi, S., Stange, G., Tensing, E., Vrekoussis, M., Bloss, W. J., Clapp, L. J., Kortner, M., Dorn, H. P., Monks, P. S., Platt, U., Plass-Dulmer, C., Mihalopoulos, N., Heard, D. E., Clemitshaw, K. C., Meixner, F. X., Prevot, A. S. H., and Schmitt, R.: Photolysis frequency measurement techniques: results of a comparison within the ACCENT project, Atmospheric Chemistry and Physics, 8, 5373-5391, 2008.

Brown, S. S., Stark, H., and Ravishankara, A. R.: Applicability of the steady state approximation to the interpretation of atmospheric observations of NO3 and N2O5, Journal of Geophysical Research-

Atmospheres, 108, Artn 4539

Doi 10.1029/2003jd003407, 2003.

Brown, S. S., Ryerson, T. B., Wollny, A. G., Brock, C. A., Peltier, R., Sullivan, A. P., Weber, R. J., Dube, W. P., Trainer, M., Meagher, J. F., Fehsenfeld, F. C., and Ravishankara, A. R.: Variability in nocturnal nitrogen oxide processing and its role in regional air quality, Science, 311, 67-70, DOI 10.1126/science.1120120, 2006.

Brown, S. S., and Stutz, J.: Nighttime radical observations and chemistry, Chem Soc Rev, 41, 6405-6447, Doi 10.1039/C2cs35181a, 2012.

Brown, S. S., Dube, W. P., Tham, Y. J., Zha, Q. Z., Xue, L. K., Poon, S., Wang, Z., Blake, D. R., Tsui, W., Parrish, D. D., and Wang, T.: Nighttime chemistry at a high altitude site above Hong Kong, Journal of Geophysical Research-Atmospheres, 121, 2457-2475, 10.1002/2015jd024566, 2016.

Chen, X., Wang, H., Lu, K., Li, C., Zhai, T., Tan, Z., Ma, X., Yang, X., Liu, Y., Chen, S., Dong, H., Li, X., Wu, Z., Hu, M., Zeng, L., and Zhang, Y.: Field Determination of Nitrate Formation Pathway in Winter Beijing, Environmental Science & Technology, 54, 9243-9253, 10.1021/acs.est.0c00972, 2020.

Chen, X., Wang, H., and Lu, K.: Interpretation of NO3–N2O5 observation via steady state in high-aerosol air mass: the impact of equilibrium coefficient in ambient conditions, Atmos. Chem. Phys., 22, 3525-3533, 10.5194/acp-22-3525-2022, 2022.

Clegg, S. L., Brimblecombe, P., and Wexler, A. S.: Thermodynamic model of the system H+-NH4+-SO42--NO3--H2O at tropospheric temperatures, J Phys Chem A, 102, 2137-2154, DOI 10.1021/jp973042r, 1998.

DeCarlo, P. F., Kimmel, J. R., Trimborn, A., Northway, M. J., Jayne, J. T., Aiken, A. C., Gonin, M., Fuhrer, K., Horvath, T., Docherty, K. S., Worsnop, D. R., and Jimenez, J. L.: Field-deployable, high-resolution, time-of-flight aerosol mass spectrometer, Analytical Chemistry, 78, 8281-8289, 10.1021/ac061249n, 2006.

Dong, H. B., Zeng, L. M., Hu, M., Wu, Y. S., Zhang, Y. H., Slanina, J., Zheng, M., Wang, Z. F., and Jansen, R.: Technical Note: The application of an improved gas and aerosol collector for ambient air pollutants in China, Atmospheric Chemistry and Physics, 12, 10519-10533, 10.5194/acp-12-10519-2012, 2012.

Eger, P. G., Friedrich, N., Schuladen, J., Shenolikar, J., Fischer, H., Tadic, I., Harder, H., Martinez, M., Rohloff, R., Tauer, S., Drewnick, F., Fachinger, F., Brooks, J., Darbyshire, E., Sciare, J., Pikridas, M., Lelieveld, J., and Crowley, J. N.: Shipborne measurements of ClNO2 in the Mediterranean Sea and around the Arabian Peninsula during summer, Atmospheric Chemistry and Physics, 19, 12121-12140, 10.5194/acp-19-12121-2019, 2019.

Evans, M. J., and Jacob, D. J.: Impact of new laboratory studies of N2O5 hydrolysis on global model budgets of tropospheric nitrogen oxides, ozone, and OH, Geophysical Research Letters, 32, Artn L09813

Doi 10.1029/2005gl022469, 2005.

Faxon, C. B., Bean, J. K., and Hildebrandt Ruiz, L.: Inland Concentrations of Cl-2 and ClNO2 in Southeast Texas Suggest Chlorine Chemistry Significantly Contributes to Atmospheric Reactivity, Atmosphere, 6, 1487-1506, 10.3390/atmos6101487, 2015.

Finlaysonpitts, B. J., Ezell, M. J., and Pitts, J. N.: Formation of Chemically Active Chlorine

793   Compounds by Reactions of Atmospheric Nacl Particles with Gaseous N2o5 and Clono2, Nature,
794   337, 241-244, Doi 10.1038/337241a0, 1989.
795   Gaston, C. J., Thornton, J. A., and Ng, N. L.: Reactive uptake of N2O5 to internally mixed inorganic
796   and organic particles: the role of organic carbon oxidation state and inferred organic phase
797   separations, Atmospheric Chemistry and Physics, 14, 5693-5707, 10.5194/acp-14-5693-2014, 2014.
798   Ghosh, B., Papanastasiou, D. K., Talukdar, R. K., Roberts, J. M., and Burkholder, J. B.: Nitryl
799   Chloride (CINO2): UV/Vis Absorption Spectrum between 210 and 296 K and O(P-3) Quantum Yield
800   at 193 and 248 nm, J Phys Chem A, 116, 5796-5805, 10.1021/jp207389y, 2012.
801   Hallquist, M., Stewart, D. J., Stephenson, S. K., and Cox, R. A.: Hydrolysis of N2O5 on sub-micron
802   sulfate aerosols, Phys Chem Chem Phys, 5, 3453-3463, Doi 10.1039/B301827j, 2003.
803   Haskins, J. D., Lee, B. H., Lopez-Hilifiker, F. D., Peng, Q. Y., Jaegle, L., Reeves, J. M., Schroder, J.
804   C., Campuzano-Jost, P., Fibiger, D., McDuffie, E. E., Jimenez, J. L., Brown, S. S., and Thornton, J.
805   A.: Observational Constraints on the Formation of Cl-2 From the Reactive Uptake of ClNO2 on
806   Aerosols in the Polluted Marine Boundary Layer, Journal of Geophysical Research-Atmospheres,
807   124, 8851-8869, 10.1029/2019jd030627, 2019.
808   He, X., Yuan, B., Wu, C., Wang, S., Wang, C., Huangfu, Y., Qi, J., Ma, N., Xu, W., Wang, M., Chen,
809   W., Su, H., Cheng, Y., and Shao, M.: Volatile organic compounds in wintertime North China Plain:
810   Insights from measurements of proton transfer reaction time-of-flight mass spectrometer (PTR-ToF-
811   MS), Journal of Environmental Sciences, 114, 98-114, https://doi.org/10.1016/j.jes.2021.08.010,
812   2022.
813   Jeong, D., Seco, R., Gu, D., Lee, Y., Nault, B. A., Knote, C. J., McGee, T., Sullivan, J. T., Jimenez, J.
814   L., Campuzano-Jost, P., Blake, D. R., Sanchez, D., Guenther, A. B., Tanner, D., Huey, L. G., Long,
815   R., Anderson, B. E., Hall, S. R., Ullmann, K., Shin, H., Herndon, S. C., Lee, Y., Kim, D., Ahn, J., and
816   Kim, S.: Integration of airborne and ground observations of nitryl chloride in the Seoul metropolitan
817   area and the implications on regional oxidation capacity during KORUS-AQ 2016, Atmos. Chem.
818   Phys., 19, 12779-12795, 10.5194/acp-19-12779-2019, 2019.
819   Le Breton, M., Hallquist, A. M., Pathak, R. K., Simpson, D., Wang, Y. J., Johansson, J., Zheng, J.,
820   Yang, Y. D., Shang, D. J., Wang, H. C., Liu, Q. Y., Chan, C., Wang, T., Bannan, T. J., Priestley, M.,
821   Percival, C. J., Shallcross, D. E., Lu, K. D., Guo, S., Hu, M., and Hallquist, M.: Chlorine oxidation
822   of VOCs at a semi-rural site in Beijing: significant chlorine liberation from ClNO2 and subsequent
823   gas- and particle-phase Cl-VOC production, Atmospheric Chemistry and Physics, 18, 13013-13030,
824   10.5194/acp-18-13013-2018, 2018.
825   Li, Q., Fu, X., Peng, X., Wang, W., Badia, A., Fernandez, R. P., Cuevas, C. A., Mu, Y., Chen, J.,
826   Jimenez, J. L., Wang, T., and Saiz-Lopez, A.: Halogens Enhance Haze Pollution in China,
827   Environmental Science & Technology, 55, 13625-13637, 10.1021/acs.est.1c01949, 2021.
828   Li, Q. Y., Zhang, L., Wang, T., Tham, Y. J., Ahmadov, R., Xue, L. K., Zhang, Q., and Zheng, J. Y.:
829   Impacts of heterogeneous uptake of dinitrogen pentoxide and chlorine activation on ozone and
830   reactive nitrogen partitioning: improvement and application of the WRF-Chem model in southern
831   China, Atmospheric Chemistry and Physics, 16, 14875-14890, 10.5194/acp-16-14875-2016, 2016.
832   Li, Q. Y., Borge, R., Sarwar, G., de la Paz, D., Gantt, B., Domingo, J., Cuevas, C. A., and Saiz-Lopez,
833   A.: Impact of halogen chemistry on summertime air quality in coastal and continental Europe:
834   application of the CMAQ model and implications for regulation, Atmospheric Chemistry and

835 Physics, 19, 15321-15337, 10.5194/acp-19-15321-2019, 2019.

836 Liu, X. G., Gu, J. W., Li, Y. P., Cheng, Y. F., Qu, Y., Han, T. T., Wang, J. L., Tian, H. Z., Chen, J., and

837 Zhang, Y. H.: Increase of aerosol scattering by hygroscopic growth: Observation, modeling, and

838 implications on visibility, Atmospheric Research, 132, 91-101, 10.1016/j.atmosres.2013.04.007,

839 2013.

840 Liu, X. X., Qu, H., Huey, L. G., Wang, Y. H., Sjostedt, S., Zeng, L. M., Lu, K. D., Wu, Y. S., Ho, M.,

841 Shao, M., Zhu, T., and Zhang, Y. H.: High Levels of Daytime Molecular Chlorine and Nitryl

842 Chloride at a Rural Site on the North China Plain, Environmental Science & Technology, 51, 9588-

843 9595, 10.1021/acs.est.7b03039, 2017.

844 Lou, S., Tan, Z., Gan, G., Chen, J., Wang, H., Gao, Y., Huang, D., Huang, C., Li, X., Song, R., Wang,

845 H., Wang, M., Wang, Q., Wu, Y., and Huang, C.: Observation based study on atmospheric oxidation

846 capacity in Shanghai during late-autumn: Contribution from nitryl chloride, Atmospheric

847 Environment, 271, 10.1016/j.atmosenv.2021.118902, 2022.

848 Lu, K. D., Rohrer, F., Holland, F., Fuchs, H., Bohn, B., Brauers, T., Chang, C. C., Haseler, R., Hu, M.,

849 Kita, K., Kondo, Y., Li, X., Lou, S. R., Nehr, S., Shao, M., Zeng, L. M., Wahner, A., Zhang, Y. H.,

850 and Hofzumahaus, A.: Observation and modelling of OH and HO2 concentrations in the Pearl River

851 Delta 2006: a missing OH source in a VOC rich atmosphere, Atmospheric Chemistry and Physics, 12,

852 1541-1569, 10.5194/acp-12-1541-2012, 2012.

853 McDuffie, E. E., Fibiger, D. L., Dube, W. P., Hilfiker, F. L., Lee, B. H., Jaegle, L., Guo, H. Y., Weber,

854 R. J., Reeves, J. M., Weinheimer, A. J., Schroder, J. C., Campuzano-Jost, P., Jimenez, J. L., Dibb, J.

855 E., Veres, P., Ebben, C., Sparks, T. L., Wooldridge, P. J., Cohen, R. C., Campos, T., Hall, S. R.,

856 Ullmann, K., Roberts, J. M., Thornton, J. A., and Brown, S. S.: ClNO2 Yields From Aircraft

857 Measurements During the 2015 WINTER Campaign and Critical Evaluation of the Current

858 Parameterization, Journal of Geophysical Research-Atmospheres, 123, 12994-13015,

859 10.1029/2018JD029358, 2018a.

860 McDuffie, E. E., Fibiger, D. L., Dube, W. P., Lopez-Hilfiker, F., Lee, B. H., Thornton, J. A., Shah, V.,

861 Jaegle, L., Guo, H. Y., Weber, R. J., Reeves, J. M., Weinheimer, A. J., Schroder, J. C., Campuzano-

862 Jost, P., Jimenez, J. L., Dibb, J. E., Veres, P., Ebben, C., Sparks, T. L., Wooldridge, P. J., Cohen, R. C.,

863 Hornbrook, R. S., Apel, E. C., Campos, T., Hall, S. R., Ullmann, K., and Brown, S. S.:

864 Heterogeneous N2O5 Uptake During Winter: Aircraft Measurements During the 2015 WINTER

865 Campaign and Critical Evaluation of Current Parameterizations, Journal of Geophysical Research-

866 Atmospheres, 123, 4345-4372, 10.1002/2018jd028336, 2018b.

867 Mentel, T. F., Sohn, M., and Wahner, A.: Nitrate effect in the heterogeneous hydrolysis of dinitrogen

868 pentoxide on aqueous aerosols, Phys Chem Chem Phys, 1, 5451-5457, Doi 10.1039/A905338g, 1999.

869 Mielke, L. H., Stutz, J., Tsai, C., Hurlock, S. C., Roberts, J. M., Veres, P. R., Froyd, K. D., Hayes, P.

870 L., Cubison, M. J., Jimenez, J. L., Washenfelder, R. A., Young, C. J., Gilman, J. B., de Gouw, J. A.,

871 Flynn, J. H., Grossberg, N., Lefer, B. L., Liu, J., Weber, R. J., and Osthoff, H. D.: Heterogeneous

872 formation of nitryl chloride and its role as a nocturnal NOx reservoir species during CalNex-LA

873 2010, Journal of Geophysical Research-Atmospheres, 118, 10638-10652, Doi 10.1002/Jgrd.50783,

874 2013.

875 Mielke, L. H., Furgeson, A., Odame-Ankrah, C. A., and Osthoff, H. D.: Ubiquity of ClNO2 in the

876 urban boundary layer of Calgary, Alberta, Canada, Canadian Journal of Chemistry, 94, 414-423,

877   10.1139/cjc-2015-0426, 2015.

878   Mozurkewich, M., and Calvert, J. G.: Reaction Probability of N2o5 on Aqueous Aerosols, Journal of

879   Geophysical Research-Atmospheres, 93, 15889-15896, DOI 10.1029/JD093iD12p15889, 1988.

880   Osthoff, H. D., Roberts, J. M., Ravishankara, A. R., Williams, E. J., Lerner, B. M., Sommariva, R.,

881   Bates, T. S., Coffman, D., Quinn, P. K., Dibb, J. E., Stark, H., Burkholder, J. B., Talukdar, R. K.,

882   Meagher, J., Fehsenfeld, F. C., and Brown, S. S.: High levels of nitryl chloride in the polluted

883   subtropical marine boundary layer, Nat Geosci, 1, 324-328, Doi 10.1038/Ngeo177, 2008.

884   Peng, X., Wang, W., Xia, M., Chen, H., Ravishankara, A. R., Li, Q., Saiz-Lopez, A., Liu, P., Zhang,

885   F., Zhang, C., Xue, L., Wang, X., George, C., Wang, J., Mu, Y., Chen, J., and Wang, T.: An

886   unexpected large continental source of reactive bromine and chlorine with significant impact on

887   wintertime air quality, Natl Sci Rev, 8, 10.1093/nsr/nwaa304, 2021.

888   Phillips, G. J., Tang, M. J., Thieser, J., Brickwedde, B., Schuster, G., Bohn, B., Lelieveld, J., and

889   Crowley, J. N.: Significant concentrations of nitryl chloride observed in rural continental Europe

890   associated with the influence of sea salt chloride and anthropogenic emissions, Geophysical

891   Research Letters, 39, Artn L10811

892   10.1029/2012gl051912, 2012.

893   Phillips, G. J., Thieser, J., Tang, M. J., Sobanski, N., Schuster, G., Fachinger, J., Drewnick, F.,

894   Borrmann, S., Bingemer, H., Lelieveld, J., and Crowley, J. N.: Estimating N2O5 uptake coefficients

895   using ambient measurements of NO3, N2O5, ClNO2 and particle-phase nitrate, Atmospheric

896   Chemistry and Physics, 16, 13231-13249, 10.5194/acp-16-13231-2016, 2016.

897   Riedel, T. P., Bertram, T. H., Crisp, T. A., Williams, E. J., Lerner, B. M., Vlasenko, A., Li, S. M.,

898   Gilman, J., de Gouw, J., Bon, D. M., Wagner, N. L., Brown, S. S., and Thornton, J. A.: Nitryl

899   Chloride and Molecular Chlorine in the Coastal Marine Boundary Layer, Environmental Science &

900   Technology, 46, 10463-10470, 10.1021/es204632r, 2012.

901   Riedel, T. P., Wagner, N. L., Dube, W. P., Middlebrook, A. M., Young, C. J., Ozturk, F., Bahreini, R.,

902   VandenBoer, T. C., Wolfe, D. E., Williams, E. J., Roberts, J. M., Brown, S. S., and Thornton, J. A.:

903   Chlorine activation within urban or power plant plumes: Vertically resolved ClNO2 and Cl-2

904   measurements from a tall tower in a polluted continental setting, Journal of Geophysical Research-

905   Atmospheres, 118, 8702-8715, 10.1002/jgrd.50637, 2013.

906   Riedel, T. P., Wolfe, G. M., Danas, K. T., Gilman, J. B., Kuster, W. C., Bon, D. M., Vlasenko, A., Li,

907   S. M., Williams, E. J., Lerner, B. M., Veres, P. R., Roberts, J. M., Holloway, J. S., Lefer, B., Brown, S.

908   S., and Thornton, J. A.: An MCM modeling study of nitryl chloride (ClNO2) impacts on oxidation,

909   ozone production and nitrogen oxide partitioning in polluted continental outflow, Atmospheric

910   Chemistry and Physics, 14, 3789-3800, 10.5194/acp-14-3789-2014, 2014.

911   Roberts, J. M., Osthoff, H. D., Brown, S. S., Ravishankara, A. R., Coffman, D., Quinn, P., and Bates,

912   T.: Laboratory studies of products of N2O5 uptake on Cl- containing substrates, Geophysical

913   Research Letters, 36, Artn L20808

914   10.1029/2009gl040448, 2009.

915   Ryder, O. S., Campbell, N. R., Shaloski, M., Al-Mashat, H., Nathanson, G. M., and Bertram, T. H.:

916   Role of Organics in Regulating ClNO2 Production at the Air-Sea Interface, J Phys Chem A, 119,

917   8519-8526, 10.1021/jp5129673, 2015.

918   Saiz-Lopez, A., and von Glasow, R.: Reactive halogen chemistry in the troposphere, Chem Soc Rev,

919   41, 6448-6472, 2012.

920   Sarwar, G., Simon, H., Xing, J., and Mathur, R.: Importance of tropospheric ClNO2 chemistry across
921   the Northern Hemisphere, Geophysical Research Letters, 41, 4050-4058, 10.1002/2014gl059962,
922   2014.

923   Shi, B., Wang, W., Zhou, L., Sun, Z., Fan, C., Chen, Y., Zhang, W., Qiao, Y., Qiao, Y., and Ge, M.:
924   Atmospheric oxidation of C10~14 n-alkanes initiated by Cl atoms: Kinetics and mechanism,
925   Atmospheric Environment, 222, 10.1016/j.atmosenv.2019.117166, 2020.

926   Simpson, W. R., Brown, S. S., Saiz-Lopez, A., Thornton, J. A., and von Glasow, R.: Tropospheric
927   Halogen Chemistry: Sources, Cycling, and Impacts, Chemical Reviews, 115, 4035-4062,
928   10.1021/cr5006638, 2015.

929   Sommariva, R., Hollis, L. D. J., Sherwen, T., Baker, A. R., Ball, S. M., Bandy, B. J., Bell, T. G.,
930   Chowdhury, M. N., Cordell, R. L., Evans, M. J., Lee, J. D., Reed, C., Reeves, C. E., Roberts, J. M.,
931   Yang, M. X., and Monks, P. S.: Seasonal and geographical variability of nitryl chloride and its
932   precursors in Northern Europe, Atmos Sci Lett, 19, UNSP e844
933   10.1002/asl.844, 2018.

934   Staudt, S., Gord, J. R., Karimova, N. V., McDuffie, E. E., Brown, S. S., Gerber, R. B., Nathanson, G.
935   M., and Bertram, T. H.: Sulfate and Carboxylate Suppress the Formation of ClNO2 at Atmospheric
936   Interfaces, Acs Earth Space Chem, 3, 1987-1997, 10.1021/acsearthspacechem.9b00177, 2019.

937   Tan, Z., Fuchs, H., Lu, K., Hofzumahaus, A., Bohn, B., Broch, S., Dong, H., Gomm, S., Haeseler, R.,
938   He, L., Holland, F., Li, X., Liu, Y., Lu, S., Rohrer, F., Shao, M., Wang, B., Wang, M., Wu, Y., Zeng,
939   L., Zhang, Y., Wahner, A., and Zhang, Y.: Radical chemistry at a rural site (Wangdu) in the North
940   China Plain: observation and model calculations of OH, HO2 and RO2 radicals, Atmospheric
941   Chemistry and Physics, 17, 663-690, 10.5194/acp-17-663-2017, 2017.

942   Tan, Z. F., Lu, K. D., Hofzumahaus, A., Fuchs, H., Bohn, B., Holland, F., Liu, Y. H., Rohrer, F., Shao,
943   M., Sun, K., Wu, Y. S., Zeng, L. M., Zhang, Y. S., Zou, Q., Kiendler-Scharr, A., Wahner, A., and
944   Zhang, Y. H.: Experimental budgets of OH, HO2, and RO2 radicals and implications for ozone
945   formation in the Pearl River Delta in China 2014, Atmospheric Chemistry and Physics, 19, 7129-
946   7150, 10.5194/acp-19-7129-2019, 2019.

947   Tang, M. J., Telford, P. J., Pope, F. D., Rkiouak, L., Abraham, N. L., Archibald, A. T., Braesicke, P.,
948   Pyle, J. A., McGregor, J., Watson, I. M., Cox, R. A., and Kalberer, M.: Heterogeneous reaction of
949   N2O5 with airborne TiO2 particles and its implication for stratospheric particle injection,
950   Atmospheric Chemistry and Physics, 14, 6035-6048, DOI 10.5194/acp-14-6035-2014, 2014.

951   Thaler, R. D., Mielke, L. H., and Osthoff, H. D.: Quantification of Nitryl Chloride at Part Per Trillion
952   Mixing Ratios by Thermal Dissociation Cavity Ring-Down Spectroscopy, Analytical Chemistry, 83,
953   2761-2766, 10.1021/ac200055z, 2011.

954   Tham, Y. J., Yan, C., Xue, L. K., Zha, Q. Z., Wang, X. F., and Wang, T.: Presence of high nitryl
955   chloride in Asian coastal environment and its impact on atmospheric photochemistry, Chinese
956   Science Bulletin, 59, 356-359, 10.1007/s11434-013-0063-y, 2014.

957   Tham, Y. J., Wang, Z., Li, Q. Y., Yun, H., Wang, W. H., Wang, X. F., Xue, L. K., Lu, K. D., Ma, N.,
958   Bohn, B., Li, X., Kecorius, S., Gross, J., Shao, M., Wiedensohler, A., Zhang, Y. H., and Wang, T.:
959   Significant concentrations of nitryl chloride sustained in the morning: investigations of the causes
960   and impacts on ozone production in a polluted region of northern China, Atmospheric Chemistry and

961   Physics, 16, 14959-14977, 10.5194/acp-16-14959-2016, 2016.

962   Tham, Y. J., Wang, Z., Li, Q. Y., Wang, W. H., Wang, X. F., Lu, K. D., Ma, N., Yan, C., Kecorius, S.,
963   Wiedensohler, A., Zhang, Y. H., and Wang, T.: Heterogeneous N2O5 uptake coefficient and
964   production yield of ClNO2 in polluted northern China: roles of aerosol water content and chemical
965   composition, Atmospheric Chemistry and Physics, 18, 13155-13171, 10.5194/acp-18-13155-2018,
966   2018.

967   Thornton, J. A., Kercher, J. P., Riedel, T. P., Wagner, N. L., Cozic, J., Holloway, J. S., Dube, W. P.,
968   Wolfe, G. M., Quinn, P. K., Middlebrook, A. M., Alexander, B., and Brown, S. S.: A large atomic
969   chlorine source inferred from mid-continental reactive nitrogen chemistry, Nature, 464, 271-274,
970   10.1038/nature08905, 2010a.

971   Thornton, J. A., Kercher, J. P., Riedel, T. P., Wagner, N. L., Cozic, J., Holloway, J. S., Dube, W. P.,
972   Wolfe, G. M., Quinn, P. K., Middlebrook, A. M., Alexander, B., and Brown, S. S.: A large atomic
973   chlorine source inferred from mid-continental reactive nitrogen chemistry, Nature, 464, 271-274,
974   10.1038/nature08905, 2010b.

975   Veres, P. R., Neuman, J. A., Bertram, T. H., Assaf, E., Wolfe, G. M., Williamson, C. J., Weinzierl, B.,
976   Tilmes, S., Thompson, C. R., Thames, A. B., Schroder, J. C., Saiz-Lopez, A., Rollins, A. W., Roberts,
977   J. M., Price, D., Peischl, J., Nault, B. A., Moller, K. H., Miller, D. O., Meinardi, S., Li, Q., Lamarque,
978   J. F., Kupc, A., Kjaergaard, H. G., Kinnison, D., Jimenez, J. L., Jernigan, C. M., Hornbrook, R. S.,
979   Hills, A., Dollner, M., Day, D. A., Cuevas, C. A., Campuzano-Jost, P., Burkholder, J., Bui, T. P.,
980   Brune, W. H., Brown, S. S., Brock, C. A., Bourgeois, I., Blake, D. R., Apel, E. C., and Ryerson, T. B.:
981   Global airborne sampling reveals a previously unobserved dimethyl sulfide oxidation mechanism in
982   the marine atmosphere, Proc Natl Acad Sci U S A, 117, 4505-4510, 10.1073/pnas.1919344117, 2020.

983   Wagner, N. L., Riedel, T. P., Roberts, J. M., Thornton, J. A., Angevine, W. M., Williams, E. J., Lerner,
984   B. M., Vlasenko, A., Li, S. M., Dube, W. P., Coffman, D. J., Bon, D. M., de Gouw, J. A., Kuster, W.
985   C., Gilman, J. B., and Brown, S. S.: The sea breeze/land breeze circulation in Los Angeles and its
986   influence on nitryl chloride production in this region, Journal of Geophysical Research-Atmospheres,
987   117, Artn D00v24
988   10.1029/2012jd017810, 2012.

989   Wahner, A., Mentel, T. F., Sohn, M., and Stier, J.: Heterogeneous reaction of N2O5 on sodium nitrate
990   aerosol, Journal of Geophysical Research-Atmospheres, 103, 31103-31112, Doi
991   10.1029/1998jd100022, 1998.

992   Wang, H., Lu, K., Chen, X., Zhu, Q., Chen, Q., Guo, S., Jiang, M., Li, X., Shang, D., Tan, Z., Wu, Y.,
993   Wu, Z., Zou, Q., Zheng, Y., Zeng, L., Zhu, T., Hu, M., and Zhang, Y.: High N2O5 Concentrations
994   Observed in Urban Beijing: Implications of a Large Nitrate Formation Pathway, Environmental
995   Science & Technology Letters, 4, 416-420, 10.1021/acs.estlett.7b00341, 2017a.

996   Wang, H., Lu, K., Tan, Z., Sun, K., Li, X., Hu, M., Shao, M., Zeng, L., Zhu, T., and Zhang, Y.: Model
997   simulation of NO3, N2O5 and ClNO2 at a rural site in Beijing during CAREBeijing-2006,
998   Atmospheric Research, 196, 97-107, 10.1016/j.atmosres.2017.06.013, 2017b.

999   Wang, H., Lu, K., Guo, S., Wu, Z., Shang, D., Tan, Z., Wang, Y., Le Breton, M., Lou, S., Tang, M.,
1000 Wu, Y., Zhu, W., Zheng, J., Zeng, L., Hallquist, M., Hu, M., and Zhang, Y.: Efficient N2O5 uptake
1001 and NO3 oxidation in the outflow of urban Beijing, Atmospheric Chemistry and Physics, 18, 9705-
1002 9721, 10.5194/acp-18-9705-2018, 2018.

1003   Wang, H., and Lu, K.: Monitoring Ambient Nitrate Radical by Open-Path Cavity-Enhanced
1004   Absorption Spectroscopy, Analytical Chemistry, 91, 10687-10693, 10.1021/acs.analchem.9b01971,
1005   2019.
1006   Wang, H., Chen, X., Lu, K., Tan, Z., Ma, X., Wu, Z., Li, X., Liu, Y., Shang, D., Wu, Y., Zeng, L., Hu,
1007   M., Schmitt, S., Kiendler-Scharr, A., Wahner, A., and Zhang, Y.: Wintertime N2O5 uptake
1008   coefficients over the North China Plain, Science Bulletin, 65, 765-774, 10.1016/j.scib.2020.02.006,
1009   2020a.
1010   Wang, H., Peng, C., Wang, X., Lou, S., Lu, K., Gan, G., Jia, X., Chen, X., Chen, J., Wang, H., Fan, S.,
1011   Wang, X., and Tang, M.: N_2O_5 uptake onto saline mineral dust: a
1012   potential missing source of tropospheric $ClNO_2$ in inland China, Atmospheric
1013   Chemistry and Physics, 22, 1845-1859, 10.5194/acp-22-1845-2022, 2022a.
1014   Wang, K., Wang, W., Fan, C., Li, J., Lei, T., Zhang, W., Shi, B., Chen, Y., Liu, M., Lian, C., Wang, Z.,
1015   and Ge, M.: Reactions of C12–C14 n-Alkylcyclohexanes with Cl Atoms: Kinetics and Secondary
1016   Organic Aerosol Formation, Environmental Science & Technology, 56, 4859-4870,
1017   10.1021/acs.est.1c08958, 2022b.
1018   Wang, T., Tham, Y. J., Xue, L. K., Li, Q. Y., Zha, Q. Z., Wang, Z., Poon, S. C. N., Dube, W. P., Blake,
1019   D. R., Louie, P. K. K., Luk, C. W. Y., Tsui, W., and Brown, S. S.: Observations of nitryl chloride and
1020   modeling its source and effect on ozone in the planetary boundary layer of southern China, Journal
1021   of Geophysical Research-Atmospheres, 121, 2476-2489, 10.1002/2015jd024556, 2016.
1022   Wang, T., Dai, J. N., Lam, K. S., Poon, C. N., and Brasseur, G. P.: Twenty-Five Years of Lower
1023   Tropospheric Ozone Observations in Tropical East Asia: The Influence of Emissions and Weather
1024   Patterns, Geophysical Research Letters, 46, 11463-11470, 10.1029/2019gl084459, 2019a.
1025   Wang, W., Yuan, B., Peng, Y., Su, H., Cheng, Y., Yang, S., Wu, C., Qi, J., Bao, F., Huangfu, Y., Wang,
1026   C., Ye, C., Wang, Z., Wang, B., Wang, X., Song, W., Hu, W., Cheng, P., Zhu, M., Zheng, J., and Shao,
1027   M.: Direct observations indicate photodegradable oxygenated volatile organic compounds (OVOCs)
1028   as larger contributors to radicals and ozone production in the atmosphere, Atmospheric Chemistry
1029   and Physics, 22, 4117-4128, 10.5194/acp-22-4117-2022, 2022c.
1030   Wang, X., Jacob, D. J., Eastham, S. D., Sulprizio, M. P., Zhu, L., Chen, Q., Alexander, B., Sherwen,
1031   T., Evans, M. J., Lee, B. H., Haskins, J. D., Lopez-Hilfiker, F. D., Thornton, J. A., Huey, G. L., and
1032   Liao, H.: The role of chlorine in global tropospheric chemistry, Atmospheric Chemistry and Physics,
1033   19, 3981-4003, 10.5194/acp-19-3981-2019, 2019b.
1034   Wang, X., Jacob, D. J., Eastham, S. D., Sulprizio, M. P., Zhu, L., Chen, Q. J., Alexander, B., Sherwen,
1035   T., Evans, M. J., Lee, B. H., Haskins, J. D., Lopez-Hilfiker, F. D., Thornton, J. A., Huey, G. L., and
1036   Liao, H.: The role of chlorine in global tropospheric chemistry, Atmospheric Chemistry and Physics,
1037   19, 3981-4003, 10.5194/acp-19-3981-2019, 2019c.
1038   Wang, X. F., Wang, H., Xue, L. K., Wang, T., Wang, L. W., Gu, R. R., Wang, W. H., Tham, Y. J.,
1039   Wang, Z., Yang, L. X., Chen, J. M., and Wang, W. X.: Observations of N2O5 and ClNO2 at a
1040   polluted urban surface site in North China: High N2O5 uptake coefficients and low ClNO2 product
1041   yields, Atmospheric Environment, 156, 125-134, 10.1016/j.atmosenv.2017.02.035, 2017c.
1042   Wang, Z., Wang, W. H., Tham, Y. J., Li, Q. Y., Wang, H., Wen, L., Wang, X. F., and Wang, T.: Fast
1043   heterogeneous N2O5 uptake and ClNO2 production in power plant and industrial plumes observed in
1044   the nocturnal residual layer over the North China Plain, Atmospheric Chemistry and Physics, 17,

1045   12361-12378, 10.5194/acp-17-12361-2017, 2017d.

1046   Wang, Z., Yuan, B., Ye, C., Roberts, J., Wisthaler, A., Lin, Y., Li, T., Wu, C., Peng, Y., Wang, C.,
1047   Wang, S., Yang, S., Wang, B., Qi, J., Wang, C., Song, W., Hu, W., Wang, X., Xu, W., Ma, N., Kuang,
1048   Y., Tao, J., Zhang, Z., Su, H., Cheng, Y., Wang, X., and Shao, M.: High Concentrations of
1049   Atmospheric Isocyanic Acid (HNCO) Produced from Secondary Sources in China, Environmental
1050   Science & Technology, 54, 11818-11826, 10.1021/acs.est.0c02843, 2020b.

1051   Wu, C., Wang, C., Wang, S., Wang, W., Yuan, B., Qi, J., Wang, B., Wang, H., Wang, C., Song, W.,
1052   Wang, X., Hu, W., Lou, S., Ye, C., Peng, Y., Wang, Z., Huangfu, Y., Xie, Y., Zhu, M., Zheng, J.,
1053   Wang, X., Jiang, B., Zhang, Z., and Shao, M.: Measurement report: Important contributions of
1054   oxygenated compounds to emissions and chemistry of volatile organic compounds in urban air,
1055   Atmos. Chem. Phys., 20, 14769-14785, 10.5194/acp-20-14769-2020, 2020.

1056   Xia, M., Peng, X., Wang, W., Yu, C., Sun, P., Li, Y., Liu, Y., Xu, Z., Wang, Z., Xu, Z., Nie, W., Ding,
1057   A., and Wang, T.: Significant production of $ClNO_2$ and possible source of
1058 Cl_2 from N_2O_5 uptake at
1059   a suburban site in eastern China, Atmospheric Chemistry and Physics, 20, 6147-6158, 10.5194/acp-
1060   20-6147-2020, 2020.

1061   Xia, M., Peng, X., Wang, W. H., Yu, C. A., Wang, Z., Tham, Y. J., Chen, J. M., Chen, H., Mu, Y. J.,
1062   Zhang, C. L., Liu, P. F., Xue, L. K., Wang, X. F., Gao, J., Li, H., and Wang, T.: Winter ClNO2
1063   formation in the region of fresh anthropogenic emissions: seasonal variability and insights into
1064   daytime peaks in northern China, Atmospheric Chemistry and Physics, 21, 15985-16000,
1065   10.5194/acp-21-15985-2021, 2021.

1066   Xue, L. K., Saunders, S. M., Wang, T., Gao, R., Wang, X. F., Zhang, Q. Z., and Wang, W. X.:
1067   Development of a chlorine chemistry module for the Master Chemical Mechanism, Geoscientific
1068   Model Development, 8, 3151-3162, 10.5194/gmd-8-3151-2015, 2015.

1069   Yang, S., Yuan, B., Peng, Y., Huang, S., Chen, W., Hu, W., Pei, C., Zhou, J., Parrish, D. D., Wang, W.,
1070   He, X., Cheng, C., Li, X.-B., Yang, X., Song, Y., Wang, H., Qi, J., Wang, B., Wang, C., Wang, C.,
1071   Wang, Z., Li, T., Zheng, E., Wang, S., Wu, C., Cai, M., Ye, C., Song, W., Cheng, P., Chen, D., Wang,
1072   X., Zhang, Z., Wang, X., Zheng, J., and Shao, M.: The formation and mitigation of nitrate pollution:
1073   comparison between urban and suburban environments, Atmospheric Chemistry and Physics, 22,
1074   4539-4556, 10.5194/acp-22-4539-2022, 2022a.

1075   Yang, X., Wang, T., Xia, M., Gao, X. M., Li, Q. Y., Zhang, N. W., Gao, Y., Lee, S. C., Wang, X. F.,
1076   Xue, L. K., Yang, L. X., and Wang, W. X.: Abundance and origin of fine particulate chloride in
1077   continental   China,   Science   of   the   Total   Environment,   624,   1041-1051,
1078   10.1016/j.scitotenv.2017.12.205, 2018.

1079   Yang, X., Wang, Q., Ma, N., Hu, W., Gao, Y., Huang, Z., Zheng, J., Yuan, B., Yang, N., Tao, J., Hong,
1080   J., Cheng, Y., and Su, H.: The impact of chlorine chemistry combined with heterogeneous
1081 N_2O_5 reactions   on   air   quality   in   China,
1082   Atmospheric Chemistry and Physics, 22, 3743-3762, 10.5194/acp-22-3743-2022, 2022b.

1083   Ye, C., Yuan, B., Lin, Y., Wang, Z., Hu, W., Li, T., Chen, W., Wu, C., Wang, C., Huang, S., Qi, J.,
1084   Wang, B., Wang, C., Song, W., Wang, X., Zheng, E., Krechmer, J. E., Ye, P., Zhang, Z., Wang, X.,
1085   Worsnop, D. R., and Shao, M.: Chemical characterization of oxygenated organic compounds in the
1086   gas phase and particle phase using iodide CIMS with FIGAERO in urban air, Atmos. Chem. Phys.,

1087   21, 8455-8478, 10.5194/acp-21-8455-2021, 2021.

1088   Young, C. J., Washenfelder, R. A., Roberts, J. M., Mielke, L. H., Osthoff, H. D., Tsai, C., Pikelnaya,
1089   O., Stutz, J., Veres, P. R., Cochran, A. K., VandenBoer, T. C., Flynn, J., Grossberg, N., Haman, C. L.,
1090   Lefer, B., Stark, H., Graus, M., de Gouw, J., Gilman, J. B., Kuster, W. C., and Brown, S. S.:
1091   Vertically Resolved Measurements of Nighttime Radical Reservoirs; in Los Angeles and Their
1092   Contribution to the Urban Radical Budget, Environmental Science & Technology, 46, 10965-10973,
1093   10.1021/es302206a, 2012.

1094   Yu, C., Wang, Z., Xia, M., Fu, X., Wang, W., Tham, Y. J., Chen, T., Zheng, P., Li, H., Shan, Y., Wang,
1095   X., Xue, L., Zhou, Y., Yue, D., Ou, Y., Gao, J., Lu, K., Brown, S. S., Zhang, Y., and Wang, T.:
1096   Heterogeneous N2O5 reactions on atmospheric aerosols at four Chinese sites: improving model
1097   representation of uptake parameters, Atmos. Chem. Phys., 20, 4367-4378, 10.5194/acp-20-4367-
1098   2020, 2020.

1099   Yun, H., Wang, T., Wang, W. H., Tham, Y. J., Li, Q. Y., Wang, Z., and Poon, S. C. N.: Nighttime NOx
1100   loss and ClNO2 formation in the residual layer of a polluted region: Insights from field
1101   measurements and an iterative box model, Science of the Total Environment, 622, 727-734,
1102   10.1016/j.scitotenv.2017.11.352, 2018a.

1103   Yun, H., Wang, W. H., Wang, T., Xia, M., Yu, C., Wang, Z., Poon, S. C. N., Yue, D. L., and Zhou, Y.:
1104   Nitrate formation from heterogeneous uptake of dinitrogen pentoxide during a severe winter haze in
1105   southern China, Atmospheric Chemistry and Physics, 18, 17515-17527, 10.5194/acp-18-17515-2018,
1106   2018b.

1107   Zhou, W., Zhao, J., Ouyang, B., Mehra, A., Xu, W. Q., Wang, Y. Y., Bannan, T. J., Worrall, S. D.,
1108   Priestley, M., Bacak, A., Chen, Q., Xie, C. H., Wang, Q. Q., Wang, J. F., Du, W., Zhang, Y. J., Ge, X.
1109   L., Ye, P. L., Lee, J. D., Fu, P. Q., Wang, Z. F., Worsnop, D., Jones, R., Percival, C. J., Coe, H., and
1110   Sun, Y. L.: Production of N2O5 and ClNO2 in summer in urban Beijing, China, Atmospheric
1111   Chemistry and Physics, 18, 11581-11597, 10.5194/acp-18-11581-2018, 2018.

1112   Zong, T., Wang, H., Wu, Z., Lu, K., Wang, Y., Zhu, Y., Shang, D., Fang, X., Huang, X., He, L., Ma,
1113   N., GroSs, J., Huang, S., Guo, S., Zeng, L., Herrmann, H., Wiedensohler, A., Zhang, Y., and Hu, M.:
1114   Particle hygroscopicity inhomogeneity and its impact on reactive uptake, The Science of the total
1115   environment, 151364-151364, 10.1016/j.scitotenv.2021.151364, 2021.

1116